ISSN 0016-7037
Volume 75, Number 1
January 1, 2011

Geochimica et Cosmochimica Acta

JOURNAL OF THE GEOCHEMICAL SOCIETY
AND THE METEORITICAL SOCIETY

Volume 75, Number 1 January 1, 2011

Articles

Continued on outside back cover

(This is a sample cover image for this issue. The actual cover is not yet available at this time.)

Available online at www.sciencedirect.com

SciVerse ScienceDirect

Geochimica et Cosmochimica Acta 78 (2012) 1–17

Geochimica et Cosmochimica Acta

www.elsevier.com/locate/gca

Evaporation and recondensation of sodium in Semarkona Type II chondrules

Roger H. Hewins [a,b,*], Brigitte Zanda [a,b], Claire Bendersky [a,c]

[a] *Laboratoire de Minéralogie et Cosmochimie du Muséum, MNHN & CNRS UMR 7202, 61 rue Buffon, 75005 Paris, France*
[b] *Earth & Planet. Sci., Rutgers University, Piscataway, NJ 08854, USA*
[c] *Lamont Doherty Earth Observatory, PO Box 1000, Palisades, NY 10964, USA*

Received 20 July 2011; accepted in revised form 10 November 2011

Abstract

We have investigated the Na distributions in Semarkona Type II chondrules by electron microprobe, analyzing olivine and melt inclusions in it, mesostasis and bulk chondrule, to see whether they indicate interactions with an ambient gas during chondrule formation. Sodium concentrations of bulk chondrule liquids, melt inclusions and mesostases can be explained to a first approximation by fractional crystallization of olivine ± pyroxene. The most primitive olivine cores in each chondrule are mostly between Fa_8 and Fa_{13}, with 0.0022–0.0069 ± 0.0013 wt.% Na_2O. Type IIA chondrule olivines have consistently higher Na contents than olivines in Type IIAB chondrules. We used the dependence of olivine–liquid Na partitioning on FeO in olivine as a measure of equilibration. Extreme olivine rim compositions are ~Fa_{35} and 0.03 wt.% Na_2O and are close to being in equilibrium with the mesostasis glass. Olivine cores compared with the bulk chondrule compositions, particularly in IIA chondrules, show very high apparent D_{Na}, indicating disequilibrium and suggesting that chondrule initial melts were more Na-rich than present chondrule bulk compositions. The apparent D_{Na} values correlate with the Na concentrations of the olivine, but not with concentrations in the bulk melt. We use equilibrium D_{Na} to find the Na content of the true parent liquid and estimate that Type IIA chondrules lost more than half their Na and recondensation was incomplete, whereas Type IIAB chondrules recovered most of theirs in their mesostases.

Glass inclusions in olivine have lower Na than expected from fractionation of bulk composition liquids, and mesostases have higher Na than expected in calculated daughter liquids formed by fractional crystallization alone. These observations also require open system behavior of chondrules, specifically evaporation of Na before formation of melt inclusions followed by recondensation of Na in mesostases. Within this record of evaporation followed by recondensation, there is no indication of a stage with zero Na in the chondrules, which is predicted by models for shock wave cooling at canonical nebular pressures, suggesting high P_T.

The high Na concentrations in olivine and mesostases indicate very high P_{Na} while chondrules were molten. This may be explained by local, very high particle densities where Type II chondrules formed. The high P_T, P_{Na} and number densities of chondrules implied suggest formation in debris clouds after protoplanetary collisions as an alternative to formation after passage of shock waves through large particle-rich clumps in the disk. Encounters of partially molten chondrules should have been frequent in these dense swarms. However, in many ordinary chondrites like Semarkona, "cluster chondrites", compound chondrules are not abundant but instead chondrules aggregated into clusters. Chondrule melting, cooling and clustering in dense swarms contributed to rapid accretion, possibly after collision, by fallback on the grandparent body and by reaccretion as a new body downrange.

* Corresponding author at: Laboratoire de Minéralogie et Cosmochimie du Muséum, MNHN & CNRS UMR 7202, 61 rue Buffon, 75005 Paris, France. Tel.: +33 1 4079 3769; fax: +33 1 4079 5772.
E-mail address: hewins@rci.rutgers.edu (R.H. Hewins).

0016-7037/$ - see front matter © 2011 Elsevier Ltd. All rights reserved.
doi:10.1016/j.gca.2011.11.027

1. INTRODUCTION

Chondrules are silicate spherules and fragments that are abundant in primitive meteorites (chondrites) and their igneous textures indicate widespread melting in the protoplanetary disk. Their formation conditions shed light on astrophysical or planetary processes occurring in the first few million years in the early solar system, and are generally consistent with transient heating mechanisms among which gas shock wave heating (Desch and Connolly, 2002) has been able to explain some chondrule properties. However, different types of chondrules experienced significant differences in their formation conditions. Type I chondrules are highly magnesian and are depleted in the moderately volatile elements, whereas Type II chondrules are ferroan and have near-chondritic abundances of the moderately volatile elements (McSween, 1977a; Scott and Taylor, 1983; Jones, 1990; Hewins, 1991). Some Type I chondrules, which are abundant in carbonaceous chondrites, contained lithic aggregates in their precursors and experienced condensation of SiO into their melts while cooling (Libourel et al., 2006; Libourel and Krot, 2007; Chaussidon et al., 2008; Whattam and Hewins, 2009). Type II porphyritic olivine and olivine–pyroxene chondrules, termed IIA and IIAB, respectively, are abundant in ordinary chondrites, and contain strongly zoned olivine phenocrysts. They appear to have formed at temperatures close to their liquidus temperatures and cooled at rates ranging from ~1 up to ~1000 °C/hr (Jones and Lofgren, 1993; Hewins et al., 2005, 2009a; Miyamoto et al., 2009). Their properties have been used to constrain chondrule formation mechanisms (Desch and Connolly, 2002; Fedkin et al., 2011).

The concentrations of moderately volatile elements in chondrule melts are the key to understanding ambient conditions during chondrule formation. Type II chondrules have chondritic abundances of moderately volatile elements, such as Na (Jones, 1990; Hewins, 1991) and show no isotopic mass fractionations, e.g. of K (Humayun and Clayton, 1995; Alexander et al., 2000). This is incompatible with free evaporation (no recondensation) as observed in experiments at canonical nebular conditions (Yu et al., 2003; Cohen et al., 2004) and suggests formation by melting in solid-enriched nebular environments (Hewins, 1989, 1991), where isotopic exchange between gas and liquid is possible (Alexander, 2004; Cuzzi and Alexander, 2006). Many chondrule glasses have close to the equilibrium compositions under conditions that could have prevented loss of Na_2O and FeO (Ebel and Grossman, 2000). Kinetic modeling shows extensive evaporation and recondensation during chondrule formation (Alexander, 2004; Fedkin et al., 2011).

Grant and Wood (2010) have studied the substitution mechanism of Na in olivine. Borisov et al. (2008) and Alexander et al. (2008a,b) recognized high Na concentrations in olivine, requiring the presence of Na in the initial chondrule melts. Evidence of either evaporation or condensation of Na in chondrules could clarify the relationship between the canonical nebular gas and a chondrule-forming environment with high P_{Na} and/or high P_{total}. Alexander et al. (2008b), using an empirical olivine-melt partition coefficient, D_{Na}, suggested that P_{Na} was very high while chondrules were molten, but argued that chondrules were essentially closed systems for Na. We take a different approach to this problem by analyzing melt inclusions in chondrules and using new, experimentally determined D_{Na} (Borisov et al., 2008; Kropf, 2009; Mathieu, 2009). We use a suite of Semarkona (LL3.0) Type II chondrules, with liquidus temperatures mostly in the range 1500–1700 °C, to determine whether Type II chondrules were open or closed systems with respect to Na when they were molten. Their olivine crystals are melt-grown, based on zoning and hopper or skeletal polyhedral morphology (Faure and Schiano, 2005; Faure et al., 2007), and on melt inclusions and mesostasis channels, which are all common (Jones, 1990, 1996; Tronche, 2007). We present analyses of chondrule minerals, mesostasis and glass inclusions in olivine to determine conditions of crystallization with emphasis on the evolution of Na concentrations during crystallization and their implications for the chondrule-forming environment.

2. METHODS

We used two Semarkona polished sections, MNHN ns1 for destructive analyses and MNHN ns2 for non-destructive work. Both were mapped in back-scattered electrons (BSE) with the JEOL 840A scanning electron microscope at the Université Paris VI. Chondrules were given the number(s) of the map image(s) which contain them. Type II porphyritic chondrules were chosen in ns2 for studies of diffusion in relict olivine grains (Hewins et al., 2009a), melt inclusions in olivine crystals (Hewins et al., 2009b), and zoning, especially of P, in olivine (Hewins, 2009). The present data are from ns2 except for some melt inclusions from below the polished surface of olivine in ns1 which were separated as fragments with a micromill.

Wavelength-dispersive quantitative analyses were made on Cameca SX100 electron microprobes at the Université Blaise Pascal in Clermont-Ferrand, and at the Université Paris VI, using 15 keV and a wide range of operating conditions. Na was always analyzed first for glasses. Conditions for Na in glass were chosen by determining the beam current for a given raster rectangle size at which Na counts from a reference region of mesostasis did not fall with time. The beam current was subsequently adapted to the size of the melt inclusion or mesostasis region to be analyzed. Common conditions were 20 s counting times and 1 nA for 1.2 μm high by 1.5 μm wide rasters (which compromised minor element precision), 2 nA for raster widths of 3 μm, 4 nA for 5 and 15 μm, and also10 nA for 5 μm. While we observed no losses with such conditions, these current densities in the range 0.02–0.55 nA/μm^2 (in reverse order) would correspond to losses of 0–5% of the amount of Na_2O present, based on analyses of an anhydrous granitic glass at 20 keV (Morgan and London, 2005). Some chondrule glasses, both inclusions and mesostases, could not be used for studies of Na partitioning because of prior high sample current work (Hewins, 2009).

Conventional electron microprobe (EMP) analyses of olivine and pyroxene were made with a focussed beam and beam currents of 10 or 30 nA with 10 s counting on peaks

and backgrounds. Beam currents of up to 300 nA and 150 s counting times were used for the olivine trace element analyses, including Na and P. This approach has been shown to give results similar to ion probe analysis (Alexander et al., 2007; Borisov et al., 2008). The combination of large diffracting crystals (LLIF and LTAP) and high beam currents ensured low detection limits, defined as 3x the background standard deviation. Cores of olivines analyzed at 300 nA for 100 s gave detection limits of 25 ppm (P), 16 ppm (Na), 50 ppm (Ca), 104 ppm (Cr) and 94 ppm (Mn). Analyses of a Na-free forsterite standard consistently yielded negative concentrations (e.g. mean −9 ppm Na_2O, s.d. 6 ppm, $n = 55$) with these conditions, confirming the observation of Kropf (2009, Fig. 12) that the curve of X-ray intensity as a function of wavelength ($\sin 2\theta$ for the TAP crystal) is concave in the vicinity of the olivine Na background. These small negative concentrations were used to correct background for each core Na_2O analysis, and they increase the Na partition coefficient by a modest 0.0001. Olivine zoning (normal, reverse, oscillatory and micron-scale) was examined with traverses with 1 μm spacing and 150 nA, as well as by X-ray mapping (Hewins, 2009). Olivine rim compositions were determined in two different ways: by 100 s single-point analyses, as for cores, where it is difficult to place the beam correctly near the rim of the crystal; and by averaging 10 s outer analyses on a traverse across a crystal, discarding the last few microns where Na and other light elements were influenced by secondary fluorescence from adjacent mesostasis. Though the detection limits for Na are poorer (73 ppm for LTAP and 143 ppm for TAP diffracting crystals) for olivine rim compositions measured on traverses, precision was improved by averaging adjacent points.

Chondrule bulk analyses were done by EMP by analyzing a grid of rastered 20 × 16 μm rectangles across the chondrule at ~70 μm spacing, with up to 80 analyses for the largest chondrule. We applied corrections for the different densities for individual phases (olivine, mesostasis, metal and sulfide in Type IIA chondrules, plus pyroxene for Type IIAB chondrules) within the analyzed volume (Warren, 1997). We calculated the abundances of FeS and Fe_xNi_{1-x} from S and Ni contents using an initial density correction using average properties of Semarkona IIA and IIAB chondrules (Jones, 1990 and Jones, 1996, respectively). The raw bulk composition data were then corrected for the densities and abundances of all phases for each chondrule.

Fractional crystallization calculations for bulk chondrule liquids were done using PETROLOG 2.1.3a (Danyushevsky, 2001; Danyushevsky and Plechov, 2011), which finds the equilibrium phase(s) at a given temperature and subtracts an increment from the liquid composition in the cooling step. Chondrules do not contain the equilibrium phase assemblage of olivine, orthopyroxene, augite and plagioclase, and both textures and SiO_2-rich glass compositions suggest rapid growth possibly associated with supercooling. Phases crystallized in a run are chosen by the user and we considered only those present in the chondrules. Supercooling is not built into the program, and the crystallization of olivine must be started at the calculated liquidus temperatures, here 1500–1717 °C. We modeled olivine crystallization alone for Type IIA chondrules, much of it metastable, and olivine plus pyroxenes for Type IIAB chondrules. For orthopyroxene we considered entry at its equilibrium temperature, delayed nucleation or total suppression. The delay of entry of orthopyroxene cannot be achieved directly in a PETROLOG run, but it can be modeled by arbitrarily choosing an intermediate/late daughter liquid resulting from metastable olivine fractionation to run as a new parent liquid.

Of more than 20 different mineral-melt equilibrium models from the literature available in PETROLOG, we used the models of Danyushevsky (2001) and Ariskin et al. (1993) for crystallization of chondrule olivine and pyroxenes, respectively, finding that they matched minor element compositions better than the others. With these phase models, olivine crystallization ceased when orthopyroxene appeared at its equilibrium temperature, and similarly orthopyroxene was followed by augite, usually with no pigeonite. When we chose intermediate/late IIAB liquids formed by crystallizing metastable olivine as new parent liquids, they crystallized pyroxenes with no olivine. We used the f_{O_2} of the Quartz–Fayalite–Iron buffer, appropriate to Type II chondrules (Zanda et al., 1994); and chose the model of Sack et al. (1980) to define melt oxidation state because it gave the lowest concentrations of Fe^{3+} in the melt, even though those concentrations are unknown. We stopped the calculations when the late liquid contained 1 wt.% MgO, yielding 12–27 wt.% residual liquid ("glass") at temperatures of 949–1068 °C. The application of MELTS to chondrules was explored at the beginning of this work and it gave results similar to those of PETROLOG.

3. RESULTS

3.1. Melt compositions

Type II chondrules found in chondritic meteorites were droplets of komatiitic liquids, in many cases totally melted, which crystallized rapidly such that plagioclase, and in some cases pyroxene, failed to nucleate, and olivine continued to crystallize metastably (e.g. McSween, 1977b; Jones, 1990). In Semarkona, Type IIA chondrules contain olivine crystals with rhyolitic glass inclusions and andesitic mesostases. Bulk compositions are shown in Table 1, along with calculated liquidus temperatures (1500–1717 °C). Our data are seen in Fig. 1a to be similar to previous analyses (Jones, 1990, 1996; Alexander et al., 2008b). Here we restrict the term IIA to chondrules that are free of pyroxene phenocrysts and designate as Type IIA(B) an olivine-dominant subset of chondrules with minor pyroxene phenocrysts. Type IIA(B) chondrules are very Mg-rich, like the Type IIAB chondrule C120 of Jones (1996), and have high liquidus temperatures (Table 1). Type IIA chondrules are the most ferroan, and pyroxene-rich IIAB chondrules have the lowest liquidus temperatures. Many phenocrysts are skeletal with glass inclusions, and apparently melt-grown, and obviously relict olivine is rare. In porphyritic chondrules, nucleation occurs on some unmelted material, but its abundance is probably small. We therefore assume that the bulk silicate composition was the initial liquid of the

Table 1
Bulk compositions (wt.%) of Semarkona Type II chondrules measured by electron microprobe.

Chondrule	6	20	98	13–36	64–65	89–90	101	21–22	99	108	4	9	51–52[b]
Type	IIA	IIA	IIA	IIA	IIA	IIA	IIA	IIA(B)	IIA(B)	IIA(B)	IIAB	IIAB	IIAB
Liq T (°C)[a]	1671	1628	1635	1632	1681	1607	1712	1633	1718	1717	1561	1500	1585
SiO_2	41.31	42.08	43.92	41.26	42.19	43.45	43.62	46.72	44.35	45.42	51.39	53.64	46.36
Al_2O_3	2.07	2.61	2.57	2.50	1.97	3.19	2.82	2.12	1.74	1.79	2.25	2.88	1.91
TiO_2	0.09	0.12	0.11	0.09	0.09	0.12	0.13	0.09	0.06	0.06	0.10	0.12	0.09
Cr_2O_3	0.64	0.78	0.43	0.57	0.42	0.58	0.69	0.69	0.51	0.72	0.78	0.67	0.66
FeO	19.34	19.43	16.39	21.19	16.82	18.61	11.64	13.43	11.86	9.31	12.27	13.46	16.08
MnO	0.45	0.45	0.36	0.38	0.37	0.39	0.51	0.44	0.36	0.51	0.49	0.51	0.52
MgO	33.55	30.97	32.49	30.95	35.18	29.73	36.47	33.75	39.17	39.72	30.16	24.81	31.63
CaO	1.50	1.93	1.87	1.89	1.51	2.11	2.05	1.76	1.01	1.61	1.78	2.29	1.81
Na_2O	0.88	1.05	1.07	0.78	0.81	1.33	1.78	0.93	0.79	0.72	0.72	1.36	0.75
K_2O	0.05	0.16	0.19	0.11	0.11	0.19	0.20	0.02	0.11	0.12	0.03	0.17	0.11
P_2O_5	0.14	0.41	0.59	0.26	0.53	0.29	0.07	0.05	0.05	0.02	0.01	0.08	0.09
Total[c]	100.00	100.00	100.00	100.00	100.00	100.00	100.00	100.00	100.00	100.00	100.00	100.00	100.00
FeS	0.61	4.23	1.85	1.98	1.22	1.87	1.20	0.30	0.57	0.48	1.16	3.04	2.69
FeNi	0.45	1.95	1.11	0.90	0.85	2.65	0.15	0.49	-0.07	0.39	0.38	1.01	1.06

[a] Liquidus temperature calculated by PETROLOG.
[b] Metal and sulfide in veins associated with fusion crust removed from analysis.
[c] S and Ni removed as sulfide and metal; silicate fraction retotalled to 100%.

chondrule, as is conventional (Jones, 1990, 1996; Alexander et al., 2008b). However, some IIA chondrule bulk compositions yield liquid lines of descent which do not reproduce the most Si-rich mesostasis compositions observed. This could be due to bulk compositions too poor in SiO_2, because the olivine/mesostasis ratio is not representative (due to a bias to crystals over mesostasis, or the presence of relict grains). Alternatively, it could be due to open system behavior, involving SiO addition from the gas, as has been demonstrated for Type I chondrules (Libourel et al., 2006) and also proposed to occur in type II chondrules (Mathieu, 2009; Villeneuve, 2010).

Analyses of glass inclusions in olivine are shown in Table 2, and of mesostasis, which consists of glass and in many cases pyroxene dendrites, in Table 3. These are shown in Fig. 1a, along with chondrule bulk compositions. In two cases, a spot in the mesostasis with composition close to stoichiometric albite was found in a chondrule which was otherwise normal. These two analyses were discarded, as albite is probably secondary (Alexander et al., 2008b). The liquid lines of descent of these chondrules were calculated using PETROLOG, assuming crystallization of olivine, and pyroxenes where appropriate. Phases which would grow at equilibrium but do not nucleate in chondrule melts (other than as fine dendrites), such as pyroxene in Type IIA chondrules, and plagioclase, were excluded from the PETROLOG calculations. In general, IIAB chondrule melts produce orthopyroxene followed by augite using the model of Ariskin et al. (1993), and rarely orthopyroxene plus pigeonite.

Fig. 1a shows our observed Al_2O_3 and Na_2O concentrations in bulk chondrules, melt inclusions and mesostases, as large symbols. The fields of corresponding data from the literature (Jones, 1990, 1996; Tronche, 2007; Alexander et al., 2008b) are shown for clarity as ellipses, not symbols. The three data sets are similar, except for variations in mesostasis analyses depending on the size of the region analyzed and the fraction of dendrites incorporated with the glass. We also show a few calculated daughter liquids as dotted and dashed liquid lines of descent, for crystallization of olivine only (IIA chondrules), and olivine followed by pyroxenes (IIAB chondrules), respectively. They stretch from the bulk compositions, their assumed parent liquids, towards the cloud of mesostasis compositions. When pyroxene is crystallized, the fractionation paths diverge to higher Na contents relative to olivine-only trends, because it removes significant Al from the liquid.

Type IIAB mesostasis is more enriched in Al and Na (and also Si) than IIA mesostasis, while melt inclusions are relatively poor in Na (Fig. 1a). The liquid lines of descent match the two mesostasis compositions fairly well, as the dashed-line trends for olivine + pyroxene crystallization for IIAB chondrules are longer than the dotted-line trends for IIA chondrules, for bulk compositions with similar Na/Al ratios. The initial Si-poor bulk compositions of IIA chondrules limit the amount of enrichment in Si and other compatible elements (Al, Na) in interstitial melt. Pyroxene crystallization enhances Al enrichment over Si enrichment of the melt in IIAB chondrules.

Melt inclusions in olivine are no more Al-enriched than Type IIA mesostases. This is because they are more highly Si-enriched than mesostases, because of more extensive metastable olivine crystallization on inclusion walls, coupled with Fe–Mg exchange between olivine and the limited melt volume. Note, however, that our melt inclusion data, almost identical to those of Tronche (2007; field 3 in Fig. 1a), have lower Na concentrations than most mesostases1 and than our calculated liquid lines of descent (Fig. 1b). The majority of the mesostases on the other hand have higher Na concentrations lying above than those same liquid lines of descent, except for the one for the most Na-rich bulk (chondrule 101).

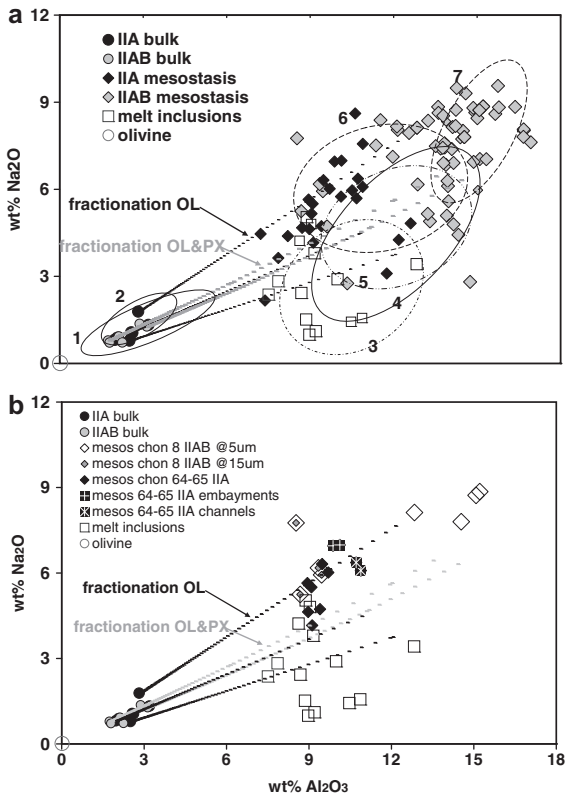

Fig. 1. Analyses of bulk compositions, melt inclusions and mesostases for Semarkona Type II chondrules with some liquid lines of descent calculated using PETROLOG. (a) Na_2O concentrations in many melt inclusions are lower, and in mesostases higher, than typical calculated daughter liquids (only chondrule 101, an exceptionally Na-rich IIAB, is able to explain most of the IIAB mesostasis, but it will explain none of the inclusions). Data from this work (symbols) and distributions from Jones (1990, 1996), Tronche (2007) and Alexander et al. (2008b), shown as numbered ellipses, are one Jones (1990, 1996) bulk compositions, two Alexander bulk compositions, three Tronche melt inclusions, four and five Jones (1990, 1996) mesostases (A, AB, respectively), six and seven Alexander mesostases (A, AB, respectively). (b) Chondrule 64–65 has a dispersion of mesostasis compositions with the highest Na for clear glass in embayments on olivine crystals and highest Al in channels inside olivine. Raster mesostasis analyses at 5 μm (open diamonds) and 15 μm (double diamonds) for chondrule 8 are Al-rich and Al-poor, and poor and rich in pyroxene dendrites, respectively.

The wide variation in the mesostasis compositions reflects fractional crystallization and perhaps open-system behavior. Therefore, in Fig. 1b we show evolution trends for observed mesostases in two specific chondrules, one IIA and one IIAB, along with the data for bulk compositions and melt inclusions. In IIA chondrule 64–65, we see a progression to higher Na contents in mesostases (which contain very fine dendrites), which correlate with higher SiO_2 contents, but with little change in Al. The most Na-rich compositions occur as clear glass in embayments touching olivine rims, showing that some olivine rims were growing from inter-dendrite melt more Na-rich than bulk mesostasis. For the Type IIAB chondrule 8 we find that smaller volumes of mesostasis are more evolved, with almost twice the Al and Na of 15 μm regions of mesostasis (Fig. 1b). They are more Na-rich than larger volumes, because of the absence of pyroxene dendrites. We assume the most Na-rich analyses of the mesostasis represent the liquid from which dendrites and the last olivine rim crystallized. We have therefore determined the apparent olivine–liquid D_{Na} relative to the most evolved mesostasis, where using possible dendrite-free interstitial glass analyzed with 5 μm rasters, rather than average mesostasis.

Liquid lines of descent for our bulk compositions cross the Al_2O_3-Na_2O field of Type II mesostasis compositions (Fig. 1), suggesting that fractionation calculations explain reasonably well the Al and Na concentrations of mesostasis. However, our bulk chondrule analyses have a small range of Na/Al ratios and many fractionation trends are concentrated together; most glass inclusions have lower Na contents than these typical calculated liquids, whereas many interstitial glasses and dendrite-rich mesostases (Fig. 1b) have higher Na contents. In detail then, the daughter liquids are not well explained by the fractionation calculations: except for one exceptionally Na-rich IIA bulk seen in Fig. 1 (chondrule 101), all Type IIA and IIAB chondrule bulks cluster together and yield liquid lines of descent that fall below most of the mesostasis points. The Na-rich bulk, in turn, will not explain the inclusions, which are all relatively Na-poor.

All model calculations have certain limitations, e.g. PETROLOG calculations involve a choice of models for mineral-melt equilibria and are for perfect fractional crystallization. However, Na and Al are essentially incompatible in olivine and low-Ca pyroxene (while augite only forms as rims on low-Ca pyroxene). Even with ~1% Al_2O_3 in orthopyroxene (PETROLOG) the liquid lines of descent are virtually straight. They are essentially just the record of the concentration of these elements in the diminishing liquid reservoir. There are no possible closed-system paths which could explain the deviations of inclusion and mesostasis compositions from the bulk liquid fractionation trends. Open-system crystallization is considered below (Section 4).

3.2. Olivine compositions

Olivine in Semarkona Type II chondrules usually shows normal zoning for most elements, but oscillatory zoning in P (McCanta et al., 2008; Hewins, 2009). Selected olivine core analyses are shown in Table 4, made using a counting time of 100 s and a beam current of 300 nA. These are the most primitive analyses for each chondrule, i.e. those with the lowest Fa and Na contents, and are used for determining D_{Na}. Na is generally present in concentrations similar to those found earlier (Borisov et al., 2008; Alexander et al., 2008b; Kropf, 2009; Mathieu, 2009), though in some chondrules it is higher. Sodium is normally zoned and, where olivine grains have reverse and then normal zoning (Jones, 1990), it follows Fa, as do other incompatible elements. In Table 5, we give analyses of olivine rims, including some alternate values obtained in different ways. Some rims were analyzed with the same conditions as the cores, giving low detection limits but not necessarily the most

Table 2
Electron microprobe analyses (wt.%) of melt inclusions in olivine in Semarkona Type II chondrules.

Chondrule	Type	SiO_2	Al_2O_3	TiO_2	FeO	Cr_2O_3	MnO	MgO	CaO	Na_2O	K_2O	P_2O_5	Total[a]
20	IIA	65.69	12.65	0.41	3.16	0.23	0.17	2.43	9.17	3.37	0.35	0.99	98.64
c31c	IIA	71.13	8.61	0.37	4.74	0.15	0.06	3.56	6.68	1.47	0.12	0.35	97.23
c31b	IIA	71.74	8.13	0.41	5.27	0.07	0.40	3.65	6.60	0.90	0.09	0.34	97.61
c31c	IIA	71.99	8.95	0.16	4.20	*0.00*	0.00	3.33	6.99	1.08	0.02	0.48	97.21
21/22	IIA(B)	74.98	10.80	0.10	1.59	0.29	0.41	1.60	7.92	1.55	0.02	0.07	99.33
21/22	IIA(B)	76.02	10.61	0.15	2.56	0.26	0.17	1.42	8.41	1.45	0.23	n.d.	101.28
99	IIA(B)	70.78	9.04	0.43	4.32	0.27	0.23	4.93	4.14	3.75	0.86	n.d.	98.76
99	IIA(B)	71.16	8.85	0.32	5.20	0.42	0.13	2.88	4.77	5.02	0.81	0.16	99.71
99	IIA(B)	74.44	10.06	0.27	2.42	0.20	0.09	2.02	7.88	2.92	0.16	0.28	100.75
99	IIA(B)	74.48	8.62	0.45	2.51	0.20	0.14	3.31	6.36	2.41	0.38	0.34	99.21
4	IIAB	71.55	9.38	0.26	2.55	0.99	0.00	7.07	6.53	0.49	0.05	n.d.	98.87
9	IIAB	78.94	8.04	0.25	3.08	0.30	0.17	1.66	6.37	2.89	0.41	0.17	102.28
9	IIAB	76.31	7.22	0.04	1.86	0.31	0.06	1.92	5.61	2.28	0.49	0.07	96.16
c22a	IIAB	75.92	9.01	0.44	3.65	0.16	0.19	3.46	0.95	4.79	0.86	0.26	99.67
c22a	IIAB	70.41	8.53	0.32	5.35	0.27	0.29	5.93	2.74	4.18	0.67	0.21	98.90

Chondrules with prefix c are from section ns1; suffices a, b, and c refer to separated fragments of these chondrules; n.d., not detected.
[a] Low totals, especially for ns1, are due to fractures related to sample extraction.

extreme compositions. In other cases, we achieved good analyses closer to the rim from traverses across crystals using 10 s and 150 nA.

Olivine core compositions were measured using 100 s and 300 nA (2 s.d. $\pm$ 0.0013 wt.% Na_2O). Sodium contents are always significantly greater than zero and are shown in Fig. 2a. The most refractory olivine cores analyzed in each chondrule, usually in the biggest crystal per chondrule, are mostly between Fa_8 and Fa_{13}, with 0.002–0.007 wt.% Na_2O (Fig. 2a). In one case where the most Fe- and Na-poor grains are not the same, both are plotted and joined by a tie line. Type IIA(B) chondrule olivines plot among the most primitive (Fe-, Ca- and Na-poor) olivines in Fig. 2a. With increasing Fa content, the IIA and IIAB trends separate, and IIA olivine cores consistently have the higher Na contents. The Fa–Ca distribution of olivine cores in IIA and IIAB chondrules is similar to that of Fa–Na, in that IIA olivine tends to have higher Ca than IIAB at the same Fa content.

In Fig. 2b we show fractionation in olivine crystal 98B, in IIA chondrule 98, the chondrule with the highest Na concentrations in olivine that we observed, along with all high resolution data for olivine cores and rims. The 98B data had counting time 10 s, beam current 150 nA, s.d. $\pm$ $\sim$0.006 wt.% Na_2O) and the data for olivine cores and rims were gathered with 100 s, 300 nA. Whereas with the higher precision we can separate IIA and IIAB olivines by Na content, here Na data spread across the two trends. Grain 98B is small and very strongly zoned. The Na fractionation is extreme in chondrule 98, but there is continuity between its crystals and trace element data for the whole suite of Type II chondrules (Fig. 2b). Zoning trends for most crystals fall near the center of the cloud of points in Fig. 2c.

Sodium zonation profiles from rim to core to rim for two crystals in chondrule 98, 98B and 98C, are shown in Fig. 3a and b the distance scale in microns from the microprobe traverse. Because of the low precision of individual 10 s analyses, some points are not significantly different from zero, though Fig. 2a shows that the average of these data is similar to the 100 s analyses, which are. Our high precision analyses of Na in chondrule olivine, and those of Borisov et al. (2008), Alexander et al. (2008a,b), are always significantly above zero. We therefore show running averages in Fig. 3a and b, with the standard deviation of the points averaged ($n = 5$) plotted as error bars. Fig. 3a also shows a more precise 100 s analysis for the core of 98B, which confirms the accuracy of the 10 s numbers. Since this core analysis is slightly off the line of the zoning traverse, we arbitrarily place it exactly in the center of the profile. Zonation profiles for Fa and Ca have similar forms to the Na profiles. The higher concentrations in the smaller crystal (98B) indicate later nucleation. The data in Fig. 2b form a single broad fractionation trend, but higher and lower Na analyses for crystal 98B with the most extreme zoning correspond to slightly different zoning trends on the two sides of the traverse (Fig. 3a); extreme rim values reflect secondary fluorescence. It is clear from Figs. 2 and 3 that ideally a large number of olivine rims should be analyzed to determine average D_{Na} for rim/mesostasis correctly.

4. DISCUSSION

4.1. Na partitioning between olivine and melt

Sodium is incompatible in olivine, because its charge is different from that of Mg yet there is no evidence of coupled substitution of Na^+ and trivalent ions for Mg in olivine (Borisov et al., 2008; Grant and Wood, 2010). Instead Grant and Wood (2010) found evidence for replacement of Mg^{2+} and a vacancy by two Na^+ ions. The situation is complicated by the competition of Li^+ with Na^+ for the vacancies, when Li is abundant.

Type II chondrules have approximately chondritic Na abundances (Hewins, 1991), which is inconsistent with formation in a canonical nebula (Yu et al., 2003; Cohen et al., 2004). Na was present in chondrule melts when olivine was crystallizing (Borisov et al., 2008; Alexander et al., 2008b; Kropf, 2009; Mathieu, 2009). The different Na concentrations preserved in Semarkona Type II chondrule bulk liquids

Table 3
Electron microprobe analyses (wt.%) of Semarkona Type II chondrule mesostases.

Chondrule	Type	Scan (μm)[a]	nA	SiO_2	Al_2O_3	TiO_2	Cr_2O_3	FeO	MnO	MgO	CaO	Na_2O	K_2O	P_2O_5	Total
20	IIA	4	10	63.99	10.88	0.53	0.15	7.77	0.10	2.24	8.26	5.81	0.88	1.41	102.02
20	IIA	4	10	62.06	10.32	0.49	0.38	7.57	0.10	4.16	9.61	5.87	0.71	0.83	102.10
55	IIA	4	10	60.18	11.14	0.52	0.49	7.55	0.18	3.90	6.75	6.93	0.28	0.14	98.05
55	IIA	4	10	59.69	11.07	0.43	0.36	6.94	0.17	4.43	7.47	7.53	0.14	0.23	98.47
64–65	IIA	15	4	57.37	9.21	0.43	0.08	12.57	0.48	3.38	6.77	4.63	0.68	2.34	97.93
64–65	IIA	15	4	53.87	8.75	0.42	2.65	13.92	0.48	4.54	5.80	4.52	0.55	2.10	97.61
64–65	IIA	15	4	53.79	8.67	0.32	0.15	13.98	0.43	6.09	6.18	3.96	0.49	1.06	95.11
64mes	IIA	25	10	55.97	8.81	0.43	0.14	13.75	0.36	3.44	6.04	5.33	0.64	2.04	96.96
64mes	IIA	5	10	58.75	9.69	0.50	0.11	10.70	0.38	1.88	9.03	6.01	0.39	2.44	99.88
64mes	IIA	25	10	58.10	9.61	0.37	0.18	13.11	0.37	3.21	7.00	6.40	0.55	2.50	101.40
64mes	IIA	25	10	57.10	9.03	0.30	0.07	14.43	0.46	3.64	7.36	5.70	0.52	2.35	100.96
64emb	IIA	5	10	59.31	10.00	0.53	0.18	10.41	0.31	2.54	7.33	7.05	0.54	3.09	101.28
64emb	IIA	5	10	59.20	10.23	0.45	0.13	10.10	0.24	2.34	7.85	7.06	0.53	2.93	101.08
64chan	IIA	5	10	60.92	10.82	0.42	0.19	9.31	0.27	2.38	7.09	6.05	0.70	1.24	99.39
64chan	IIA	5	10	60.76	10.87	0.43	0.17	9.45	0.41	1.87	9.15	6.46	0.72	1.16	101.43
89–90	IIA	15	4	55.08	8.16	0.46	0.40	11.34	0.38	12.17	6.02	4.37	0.59	0.61	99.57
89–90	IIA	15	4	52.20	7.18	0.33	1.97	12.60	0.28	14.71	4.63	4.44	0.42	0.67	99.43
89–90	IIA	15	4	56.79	8.96	0.44	0.53	9.57	0.37	9.93	5.95	5.11	0.58	0.75	98.97
89–90	IIA	15	4	55.94	8.67	0.34	0.46	10.52	0.36	11.24	5.80	4.65	0.60	0.96	99.55
98	IIA	15	4	63.36	10.57	0.50	0.12	9.72	0.32	2.37	4.68	3.50	0.96	1.39	97.50
98	IIA	4	10	64.43	11.96	0.47	0.03	9.14	0.21	1.62	3.80	4.18	0.75	1.55	98.14
98	IIA	4	10	66.96	12.39	0.43	0.03	9.02	0.14	0.62	1.50	4.74	0.97	1.47	98.27
98	IIA	4	10	64.13	10.65	0.49	n.d.	11.10	0.39	1.19	1.25	8.63	1.29	1.15	100.25
98	IIA	4	10	62.94	10.47	0.58	0.08	8.69	0.32	2.69	5.54	5.94	0.80	1.60	99.65
98	IIA	4	10	62.73	10.89	0.41	0.09	9.45	0.27	2.16	4.13	7.56	0.77	1.50	99.96
122	IIA	15	4	50.55	8.95	0.38	0.09	10.69	0.28	7.17	7.43	5.62	0.09	2.04	93.30
122	IIA	15	4	62.06	11.52	0.56	0.14	7.46	0.12	3.18	7.01	3.04	0.92	2.00	98.01
122	IIA	15	4	52.00	7.70	0.39	0.29	14.34	0.40	10.92	6.30	3.56	0.64	1.48	98.03
21/22	IIA(B)	4	10	65.50	16.16	0.49	0.03	4.03	0.15	0.81	2.10	9.89	0.11	0.22	99.48
21/22	IIA(B)	4	10	62.91	15.96	0.67	0.07	5.96	0.23	1.01	2.66	9.53	0.02	0.22	99.22
99	IIA(B)	4	10	65.71	13.73	0.47	0.05	6.92	0.16	0.98	1.67	8.24	0.72	0.22	98.86
99	IIA(B)	4	10	66.90	14.27	0.35	0.11	5.48	0.24	0.99	1.79	7.66	1.01	0.28	99.09
99	IIA(B)	4	10	69.64	14.94	0.53	0.06	4.22	0.12	1.33	1.31	5.93	1.05	0.25	99.38
c31a	IIA(B)	1.5	1	75.89	14.23	0.25	n.d.	3.87	0.29	0.07	0.75	5.69	0.72	0.07	101.82
c31a	IIA(B)	1.5	1	70.68	15.23	0.72	0.04	4.31	n.d.	0.29	1.14	7.10	0.87	0.49	100.88
c31c	IIA(B)	1.5	1	70.33	13.94	0.51	0.14	4.41	0.06	0.13	0.52	6.81	1.32	0.35	98.51
c31c	IIA(B)	1.5	1	64.62	14.50	0.04	n.d.	5.48	n.d.	0.52	1.59	6.66	1.13	0.03	94.57
c31c	IIA(B)	1.5	1	71.72	14.01	0.76	0.02	3.88	0.40	0.32	0.84	4.33	1.31	0.17	97.75
c31b	IIA(B)	3	2	72.66	13.99	0.65	n.d.	4.21	0.12	0.35	0.65	7.53	1.01	n.d.	101.16
c31b	IIA(B)	3	2	72.96	12.38	0.58	n.d.	3.16	0.29	0.67	0.76	7.06	1.18	0.17	99.23
c31b	IIA(B)	3	2	72.69	12.47	0.52	0.29	2.58	0.00	0.64	0.63	5.98	0.81	0.34	96.95
c31c	IIA(B)	3	2	72.18	14.45	0.48	0.29	4.84	0.17	0.18	0.99	7.57	0.84	0.52	102.52
c31a	IIA(B)	1	10	69.82	13.76	0.46	0.06	6.39	0.13	0.11	0.60	6.03	1.09	0.16	98.59
c31a	IIA(B)	1	10	62.50	10.58	0.54	0.03	11.91	0.37	1.62	5.22	4.64	0.82	0.20	98.43
c31c	IIA(B)	1	10	68.77	13.79	0.38	0.11	5.74	0.14	1.07	2.88	5.05	0.99	0.20	99.12
c31c	IIA(B)	1	10	70.98	13.36	0.64	n.d.	5.90	0.20	0.98	2.59	5.21	0.98	0.22	101.04
4	IIAB	4	10	58.20	16.30	0.64	0.02	9.82	0.46	1.78	5.34	8.40	0.22	0.05	101.21
4	IIAB	4	10	60.52	16.61	0.78	n.d.	7.68	0.31	1.81	5.67	8.60	0.34	n.d.	102.32
4	IIAB	5	4	58.28	17.35	0.50	0.04	10.46	0.48	1.58	5.52	7.81	0.22	0.23	102.47
4	IIAB	5	4	61.16	17.13	0.55	0.13	7.52	0.30	1.93	5.63	8.29	0.06	0.06	102.77
4	IIAB	5	4	61.19	17.12	0.72	0.07	6.48	0.35	2.06	6.36	8.02	0.31	0.06	102.76
4	IIAB	5	1	72.40	10.56	0.82	0.60	3.07	n.d.	3.99	7.70	2.82	0.23	n.d.	102.18
4	IIAB	3	1	66.01	8.94	0.63	0.56	2.56	0.41	3.91	4.98	4.39	0.66	n.d.	93.04
8	IIAB	5	4	69.02	14.68	0.47	n.d.	5.16	0.17	0.66	1.81	7.88	0.87	0.26	100.98
8	IIAB	5	4	67.37	15.65	0.54	0.01	5.65	0.17	0.85	2.23	9.11	0.91	0.37	102.85
8	IIAB	5	4	71.18	15.43	0.44	0.05	3.50	0.07	0.63	0.69	8.93	1.03	0.37	102.32
8	IIAB	5	4	72.72	13.05	0.45	0.00	5.31	0.03	0.38	0.49	8.26	0.92	0.04	101.67
8	IIAB	15	4	64.05	9.38	0.46	7.40	0.59	0.26	4.39	6.03	5.89	0.67	0.08	99.20
8	IIAB	15	4	62.40	8.62	0.46	8.04	0.66	0.43	5.23	7.25	5.21	0.72	0.29	99.31
8	IIAB	15	4	64.87	9.34	0.43	7.29	0.58	0.31	4.28	5.81	6.18	0.79	0.06	99.93
9	IIAB	4	10	62.90	11.98	0.52	n.d.	13.64	0.32	0.65	0.19	8.19	0.94	0.23	99.57
9	IIAB	4	10	65.85	14.10	0.39	0.05	9.54	0.21	0.27	0.44	8.24	0.89	0.26	100.24
9	IIAB	4	10	66.38	12.49	0.51	0.03	11.60	0.38	0.68	1.38	7.89	0.84	0.31	102.47

(*continued on next page*)

Table 3 (*continued*)

Chondrule	Type	Scan (μm)[a]	nA	SiO_2	Al_2O_3	TiO_2	Cr_2O_3	FeO	MnO	MgO	CaO	Na_2O	K_2O	P_2O_5	Total
9	IIAB	5	4	68.16	11.62	0.39	0.06	8.23	0.20	1.52	0.54	8.45	0.82	0.84	100.83
9	IIAB	5	4	67.01	12.21	0.51	0.07	11.11	0.29	0.98	1.59	7.27	0.73	0.26	102.02
9	IIAB	5	4	65.39	12.64	0.54	0.07	10.51	0.34	0.68	1.37	8.00	0.75	0.43	100.69
9	IIAB	5	4	68.13	12.30	0.50	0.05	9.54	0.26	0.71	0.59	8.29	0.90	0.24	101.52
9	IIAB	1.5	1	69.29	13.11	0.45	n.d.	8.45	0.11	1.06	0.32	4.83	0.74	0.17	98.55
9	IIAB	1.5	1	69.26	11.45	0.09	n.d.	8.58	n.d.	1.42	0.46	7.57	0.68	1.27	100.79
51/52	IIAB	4	10	67.97	15.29	0.43	0.05	4.16	0.12	1.55	0.40	5.78	1.04	0.06	96.86
51/52	IIAB	1.5	1	67.35	16.83	0.87	0.15	4.64	0.06	1.14	0.44	8.10	1.25	0.07	100.90
51/52	IIAB	1.5	1	67.23	14.36	0.72	0.02	4.92	0.46	1.57	0.30	7.94	1.15	0.42	99.09
71–72	IIAB	5	4	64.81	13.88	0.62	0.33	5.26	0.32	2.75	4.93	6.95	0.76	0.02	100.64
71–72	IIAB	5	4	65.42	15.68	0.47	0.03	4.18	0.25	1.22	2.47	8.77	0.81	0.04	99.35
71–72	IIAB	5	4	65.38	15.20	0.60	0.07	4.14	0.29	2.25	3.92	8.56	0.84	0.02	101.28
72only	IIAB	5	4	67.02	13.80	0.51	0.07	7.60	0.41	1.72	2.31	7.65	0.81	0.21	102.13
72only	IIAB	5	4	65.55	13.89	0.40	0.16	7.82	0.48	1.85	2.53	7.50	0.76	n.d.	100.95
137	IIAB	5	4	67.21	14.68	0.51	0.06	5.80	0.25	1.29	0.62	9.37	0.87	0.02	100.67
137	IIAB	5	4	63.49	14.49	0.55	0.04	7.52	0.54	1.95	4.20	8.34	0.73	0.04	101.90
137	IIAB	5	4	65.48	16.68	0.56	0.07	5.75	0.18	1.06	2.20	9.01	0.88	0.02	101.89
137	IIAB	5	4	63.16	14.03	0.59	0.09	7.86	0.35	2.06	4.86	7.70	0.77	0.00	101.45
137	IIAB	5	4	67.69	14.24	0.55	0.12	10.18	0.35	0.62	1.21	4.82	0.82	0.02	100.61
c22a	IIAB	3	3	68.19	13.68	0.48	0.01	6.44	0.22	1.01	0.78	8.68	0.89	0.15	100.52
c22a	IIAB	3	*3*	69.03	13.75	0.43	n.d.	6.48	0.28	0.56	0.63	8.93	1.01	0.00	101.09
c22a	IIAB	3	3	66.93	15.49	0.52	n.d.	4.17	0.16	1.14	0.79	8.51	0.96	0.26	98.93
c22a	IIAB	3	*3*	69.30	14.99	0.47	0.02	4.07	0.16	0.69	0.55	6.85	0.98	0.11	98.17
c22a	IIAB	3	3	69.66	12.22	0.64	0.01	6.39	0.25	1.36	0.76	8.10	1.02	0.24	100.64
c22a	IIAB	3	*3*	69.54	14.14	0.40	n.d.	4.76	0.27	1.14	0.56	8.16	1.07	0.09	100.13
c22a	IIAB	3	3	71.40	14.06	0.61	0.03	4.28	0.16	1.13	0.47	4.51	1.14	0.17	97.97
c22a	IIAB	3	*3*	70.32	15.06	0.55	0.05	5.26	0.28	0.82	0.65	6.97	1.09	0.15	101.19
c22a	IIAB	3	2	68.67	13.05	0.59	0.20	4.22	0.20	1.63	0.62	8.24	1.07	0.09	98.58
c22a	IIAB	3	2	69.31	14.45	0.61	0.07	4.33	0.12	1.98	0.66	7.81	1.17	0.17	100.68
c22a	IIAB	3	2	66.56	14.24	0.51	0.13	4.82	0.19	2.80	1.00	8.74	0.81	0.21	100.03
c22a	IIAB	3	2	68.81	11.83	0.57	0.05	3.73	0.39	2.85	0.65	7.41	1.18	0.51	98.90
c22a	IIAB	3	2	66.53	14.60	0.54	n.d.	5.26	0.11	0.96	0.89	8.65	0.68	n.d.	97.97
c22a	IIAB	3	2	69.27	13.58	0.53	n.d.	3.17	0.06	1.11	0.67	8.41	1.20	0.52	98.23
c22a	IIAB	3	2	68.53	16.25	0.51	n.d.	5.96	0.34	0.55	0.28	9.86	0.71	0.17	103.15
c22a	IIAB	1.5	1	72.09	13.85	n.d.	n.d.	4.23	n.d.	1.69	0.10	6.83	0.85	0.18	99.81
c22a	IIAB	1.5	1	67.33	13.35	0.46	n.d.	5.87	0.29	0.91	0.61	7.22	1.28	0.21	97.52
c22a	IIAB	1.5	1	68.68	14.58	n.d.	0.07	3.17	0.35	1.16	0.59	8.44	0.53	0.07	97.64
c22b	IIAB	3	2	65.53	13.87	0.62	0.22	2.55	0.12	2.12	1.21	9.23	1.25	0.52	97.24
c8/21c	IIAB	3	2	62.86	10.53	0.49	n.d.	6.90	0.23	1.78	4.10	8.92	0.55	0.86	97.23

Chondrules with prefix c are from section ns1; suffices a, b, and c refer to separated fragments of these chondrule; n.d., not detected.
[a] Raster width.

Table 4
Most primitive olivine core compositions (wt.%) measured by electron microprobe in Semarkona Type II chondrules.

Chondrule	Type	SiO_2	Cr_2O_3	FeO	MnO	MgO	CaO	Na_2O	P_2O_5	Total	Fa	∑cat	Si
6B	IIA	39.89	0.42	11.00	0.24	48.44	0.10	0.0055	0.017	100.12	11.30	2.03	0.99
13–36C	IIA	39.32	0.44	15.04	0.26	44.74	0.11	0.0102	0.078	100.00	15.87	2.01	0.99
20	IIA	39.73	0.39	11.74	0.25	47.92	0.10	0.0067	0.022	100.17	12.09	2.03	0.98
64–65	IIA	39.87	0.34	11.91	0.22	47.68	0.10	0.0069	0.035	100.17	12.29	2.03	0.99
89–90 C	IIA	41.17	0.31	9.55	0.20	49.50	0.10	0.0067	0.060	100.89	9.77	2.00	1.00
98B	IIA	38.84	0.47	16.28	0.33	43.76	0.13	0.0140	0.140	99.97	17.27	2.02	0.99
101	IIA	40.45	0.52	8.62	0.27	50.05	0.09	0.0044	0.013	100.03	8.81	2.01	0.99
21–22	IIA(B)	39.50	0.54	11.10	0.29	48.13	0.11	0.0030	0.004	99.67	11.45	2.03	0.98
99	IIA(B)	40.30	0.40	9.40	0.25	49.66	0.08	0.0058	0.015	100.11	9.60	2.02	0.99
108	IIA(B)	40.58	0.59	8.56	0.35	49.73	0.09	0.0022	0.009	99.90	8.80	2.02	0.99
4	IIAB	39.27	0.44	10.14	0.27	49.23	0.07	0.0026	0.007	99.43	10.36	2.05	0.97
9	IIAB	39.44	0.46	15.31	0.41	44.23	0.07	0.0053	0.038	99.96	16.26	2.00	1.00
51–52	IIAB	39.70	0.48	11.21	0.30	47.80	0.08	0.0027	0.009	99.57	11.63	2.02	0.99
Det. Lim.	300 nA	100s	0.010		0.009		0.005	0.0016	0.0025				

Standard deviation from counting statistics 0.0006 wt.% Na_2O.

Table 5
Rim olivine compositions (wt.%) measured by electron microprobe in Semarkona Type II chondrules.

Chondrule	Type	SiO_2	Al_2O_3[a]	Cr_2O_3	FeO	MnO	MgO	CaO	Na_2O	Na s.d.[b]	DetLim	P_2O_5	Total	∑cations	Si	Fa
64–65	IIA	37.95		0.56	22.86	0.50	36.59	0.20	0.0220	0.0059	0.0076	0.033	98.69	1.98	1.01	25.99
89–90	IIA	37.79	0.032	0.45	24.86	0.59	35.30	0.27	0.0195	0.0012	0.0143	0.084	99.39	1.98	1.01	28.34
89–90	IIA	38.71		0.54	22.18	0.50	38.21	0.25	0.0191	*0.0016*	0.0016	0.222	100.63	1.98	1.00	24.56
98	IIA	37.84	0.027	0.51	20.68	0.44	39.00	0.21	0.0260	0.0065	0.0143	0.134	98.89	2.01	0.99	22.97
122	IIA	36.43	0.028	0.34	30.03	0.56	30.95	0.35	0.0228	0.0023	0.0143	0.163	98.91	1.99	1.00	35.27
122	IIA	37.15		0.42	25.17	0.50	35.60	0.24	0.0153	*0.0016*	0.0016	0.066	99.16	2.01	0.99	28.40
8	IIA(B)	36.99	0.051	0.63	23.71	0.65	36.31	0.23	0.0164	0.0013	0.0143	0.023	98.64	2.01	0.99	26.82
99	IIA(B)	38.85		0.51	19.72	0.53	40.18	0.18	0.0140	*0.0015*	0.0016	0.025	100.01	1.99	1.00	21.59
51–52	IIAB	38.11		0.50	22.00	0.73	37.59	0.19	0.0175	*0.0020*	0.0016	0.024	99.17	1.99	1.00	24.72

[a] Analyses with Al and 64–65 had 10 s counting time; others without Al had 100 s counting time, and usually no replicates.
[b] s.d. is standard deviation of analyses averaged or, where no replicates, error from counting statistics shown in italics.

and mesostases only approximate what can be explained by fractional crystallization (Fig. 1a). Most glass inclusions in olivine have lower Na than it predicts and most mesostases have higher Na. It is plausible that the decrease results from early evaporation, evidence of which was preserved only in melt enclosed in olivine, and that the increase results from later condensation of Na from the ambient gas during cooling. In this case, the initial Na concentration in the liquid was not the current bulk Na concentration. Fractional crystallization of olivine changes liquid structure as well as composition, and increases its Na solubility (Mathieu, 2009), so it is possible that ambient P_{Na} could have varied relatively little. Na partitioning data (Borisov et al., 2008; Alexander et al., 2008b; Kropf, 2009; Mathieu, 2009) can permit us to determine if olivine and melt were in equilibrium, and potentially confirm that the chondrule melt was experiencing evaporation and condensation, in turn giving an idea of P_{Na} when the chondrules melted and cooled.

Fig. 4 shows the concentration of Na_2O in most primitive olivine cores and most ferroan rims plotted against the Na_2O in bulk liquids and mesostases, respectively, considering the assumption of Alexander et al. (2008b) that these may be equilibrium pairs. This would be the case for perfect fractional crystallization of a complete liquid, though we discuss below whether this assumption is justified. The rim and especially the core data have a wide spread rather than a linear trend corresponding to a constant distribution coefficient in Fig. 4. As D_{Na} olivine/melt is thought to depend on olivine FeO content (Borisov et al., 2008; Kropf, 2009; Mathieu, 2009), we also show curves for olivine-melt equilibrium for three specific olivine FeO contents, based on the relationship determined by Mathieu (2009). Olivine rims, with 20–30 wt.% FeO, fall across the region determined for 10–30 wt.% FeO in olivine, and especially those for IIA chondrules are close to being in equilibrium with the melt (mesostasis). However, most of the core-bulk pairs, with 8–16 wt.% FeO in olivine, lie beyond the line for 20% FeO in olivine (and even the 30% one). The Type IIA olivine cores, in particular, are far from being in equilibrium.

It is possible that the Semarkona Type II olivine cores do not have compositions produced by fractional crystallization, but have approached equilibrium with the bulk liquid, by diffusion of Fe, Mg, Ca, Na, etc. Values for the diffusion coefficient for Na in olivine are similar to those for Ca, and overlap those for Fe–Mg (Spandler and O'Neill, 2010). Observed Fe–Mg zoning profiles in Type II olivine show a mismatch to profiles calculated by fractional crystallization models (e.g. Jones, 1990; Miyamoto et al., 2009) probably due to diffusional modification. Miyamoto et al. (2009) modeled the diffusional modification of olivine Fe–Mg profiles and extracted chondrule cooling rates. Then the composition of the cores, including minor and trace elements, if modified by exchange with liquid, might be approximately in equilibrium with a somewhat evolved liquid. To illustrate this effect, we used PETROLOG to calculate the composition of interstitial liquids after 50% olivine had been crystallized, and compared the olivine core Na_2O concentrations, assumed for this purpose not to be the as-solidified compositions, with the 50% liquid Na_2O concentrations. Fig. 4 shows that these composition pairs would be much closer to the equilibrium curves. However, the failure of diffusion to destroy relict forsteritic cores raises doubt that Na diffusion would have been fast enough to raise Na concentrations in olivine cores and explain the apparent departure from equilibrium (though see below).

In the absence of a simple relationship between Na in olivine and Na in liquid, at least for the olivine core/bulk composition pairs, we re-examine the possible dependence of the partition coefficient on the FeO content of the olivine (Kropf, 2009; Mathieu, 2009). D_{Ca} olivine/melt is strongly dependent on Fe content (Libourel, 1999). Both studies of Na partitioning (Kropf, 2009; Mathieu, 2009) involved experiments in the FeO-free systems and led to values which are similar (Fig. 5a). Grant and Wood (2010) also measured D_{Na}(Fo/Liq) bur found a wide range of values related to the Li/Na ratios of the liquids and the inferred competition for vacancies. Kropf (2009) and Mathieu (2009) developed expressions for the FeO dependence of D_{Na}. This dependence is not well constrained, being based partly on chondrules and, in the case of Kropf (2009), a single experimental study with ferroan compositions (Borisov et al., 2008), in which P_{Na} decreased with time during runs, or in the case of Mathieu (2009), terrestrial rocks. Furthermore the charges of Borisov et al. (2008) with 6–13 wt.% FeO in olivine do not show a significant correlation between

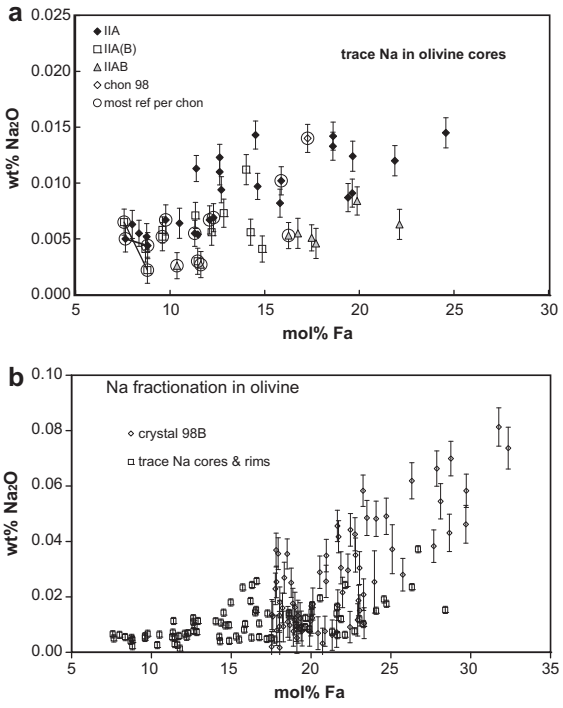

Fig. 2. (a) Fayalite and Na contents of olivine crystals from Semarkona Type II chondrules. Core compositions measured with 300 nA and 100 s counting time for trace elements. Type IIA have higher Na than Type IIAB. Errors bars are 2 s.d. of counting statistics, on average ±0.0013 wt.% Na_2O. (b) Fayalite and Na contents of olivine crystals from Semarkona Type II chondrules. Trace element data (100 s counting) for cores and rims compared to zoning profile data (10 s counting) for crystal B in chondrule 98, the chondrule with the most Na-rich olivine. Errors bars for 98B are 2 s.d. of counting statistics, on average ±0.006 wt.% Na_2O.

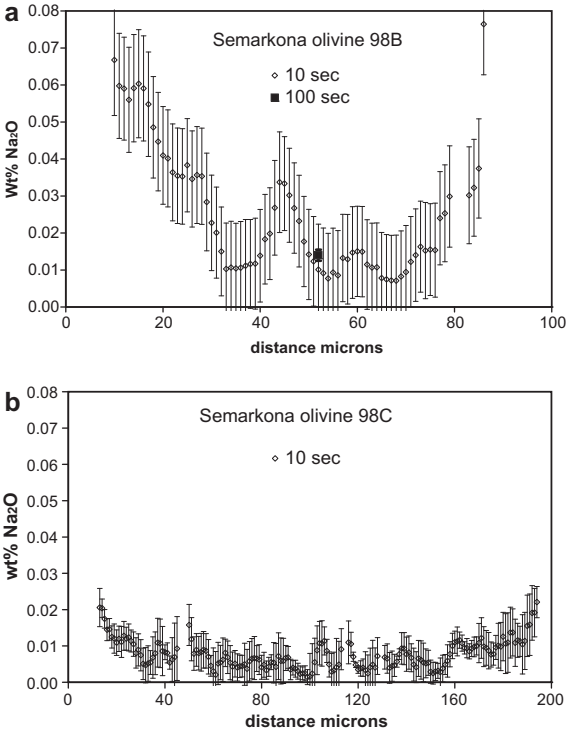

Fig. 3. Na zoning profiles rim–core–rim for crystals B and C in chondrule 98. Because of the low precision with 10 s counting times, these are running-averaged data ($n = 5$) and the standard deviations of the points analyzed are used as error bars. (a) Grain 98B (core Fa_{18}) has the most extreme Na zoning measured. The core Na concentration in 98B determined by trace element techniques is placed at the center of the profile. (b) Grain 98C (core Fa_{12}) nucleated earlier than 98B.

FeO and D_{Na} (Fig. 5a). It is difficult to evaluate chondrule equilibrium with respect to Na with a calibration largely based on chondrule data, especially as we have shown above that there are doubts that we can identify equilibrium pairs. However, the relationship of Mathieu (2009), $D_{Na} = 0.0011 + 0.00011*FeO$ (wt.%), passes through data for olivine in oceanites and boninites, where evaporation and condensation are not an issue. In addition, the D_{Na} of Alexander et al. (2008b), based on microphenocrysts in chondrule glass, falls just above the value predicted by this curve (Fig. 5a). Therefore we consider this D_{Na}–FeO relationship (Mathieu, 2009) as the best guide to olivine-melt equilibrium in chondrules.

In Fig. 5b we explore the apparent D_{Na}–FeO relationships for Semarkona Type II chondrules, using our data (Table 6) and those of Alexander et al. (2008b). Our results for olivine rims/mesostasis fall below the FeO dependence curve of Kropf (2009) and close to that of Mathieu (2009). The olivine rims analyzed in this study and those of Alexander et al. (2008a) are clearly close to being in equilibrium with mesostasis. Assuming the most primitive olivine cores coexisted with melt of bulk chondrule composition, most IIAB olivine cores (round symbols *without* black dots) also appear to be in equilibrium. Other olivine cores analyzed by us and by Alexander et al. (2008b), particularly in IIA chondrules (black dot symbols), have very high apparent D_{Na}, which is incompatible with forma-

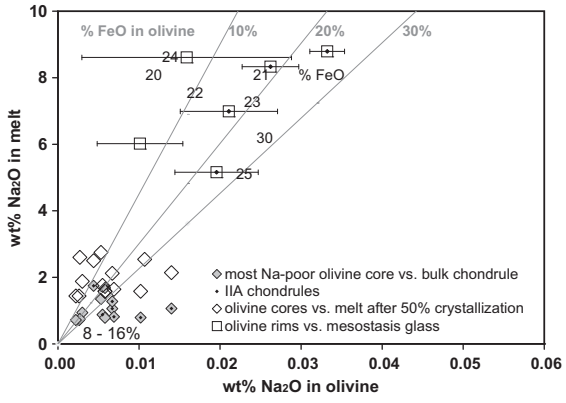

Fig. 4. Na concentrations in olivine (cores and rims) and coexisting melts (bulk compositions and mesostasis glass, respectively). Equilibrium partitioning as a function of olivine FeO (Mathieu, 2009) is shown as diagonal lines. Olivine rims are close to equilibrium, but many cores, especially in Type IIA chondrules, are not. Such cores would be closer to equilibrium with more Na-rich melts, e.g. those shown which have crystallized 50% olivine.

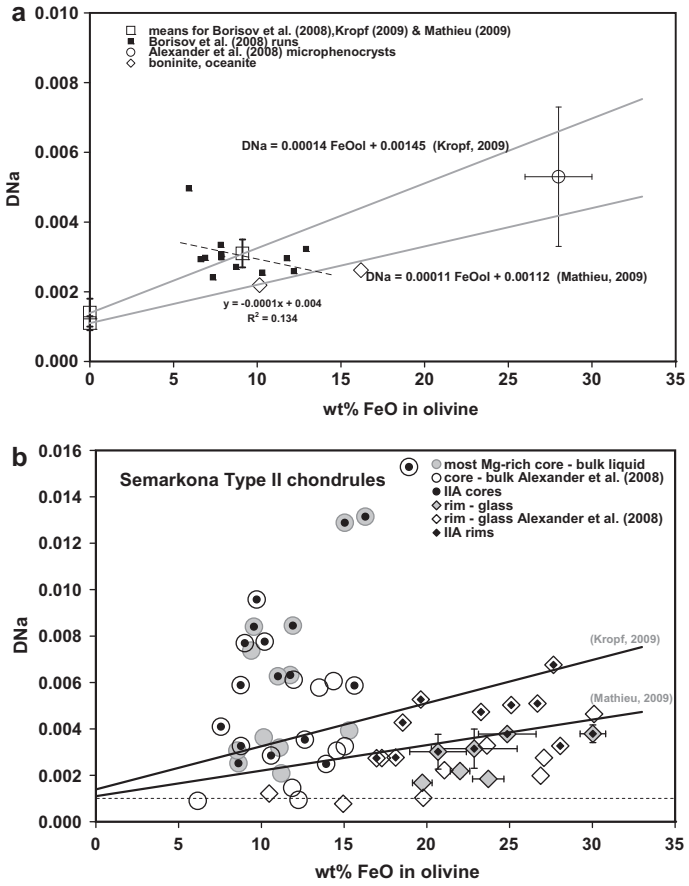

Fig. 5. Partitioning of Na between olivine and melt, and the effect of olivine FeO content on partition coefficient. (a) Experimental results of Borisov et al. (2008), Kropf (2009) and Mathieu (2009); boninite and oceanite data from Mathieu (2009). (b) Data for Type II chondrules from this work and Alexander et al. (2008b). Rims are close to equilibrium. Some cores, especially in Type IIA chondrules, are far from equilibrium. Dashed line – no Fe dependence.

tion of olivine core compositions from the observed bulk liquid at equilibrium, as shown in Fig 4. Note that some data in Fig. 5b, especially for IIAB olivine rims, fall below the equilibrium curve and close to the horizontal dashed line, corresponding to no dependence of D_{Na} on olivine FeO.

Fig. 5b shows that both cores and rims of Type IIA chondrule olivine have higher D_{Na} than cores and rims of Type IIAB chondrule olivine, respectively, for both our data and those of Alexander et al. (2008b). The exceptionally high D_{Na} for some Type IIA olivine cores means that either the olivine has anomalously high Na concentrations or the bulk liquid has anomalously low Na concentrations. Comparison of the analyses for Type IIA and other chondrules shows that the former is the case: IIA bulk compositions (Table 1) are not significantly different from Type IIA(B) and IIAB bulks (mean 1.10 wt.% Na_2O, s.d. 0.35 for IIA vs. 0.97 wt.% Na_2O, s.d. 0.28 for the others); a *t*-test shows that IIA olivine core Na_2O (0.0083 wt.%, s.d. 0.0034) is different at the 95% confidence level from IIA(B) and IIAB olivine core Na (0.0036 wt.%, s.d. 0.0015).

The correlation expected between core olivine Na and bulk melt Na, if at equilibrium, is not observed (Fig. 4). There is a strong dependence ($R^2 = 0.77$) of D_{Na} values for primitive olivine cores on the Na concentration of the olivine (Fig. 6a), whereas there is no significant negative correlation ($R^2 = 0.23$) with bulk liquid compositions (Fig. 6b). Similarly there are no correlations between D_{Na} and other liquid composition parameters or liquidus temperature. In the case of a correlation of D_{Na} with liquid Na but not with olivine Na, contents we could have argued that the apparent D_{Na} was increased by inward diffusion from a liquid relatively enriched in Na. However, the apparent departure from equilibrium partitioning is clearly due to incorporation of high concentrations of Na in the olivine cores, suggesting formation from an initial liquid later depleted in Na, assuming that diffusion of Na into olivine cores is not important.

4.2. Na diffusion

Zoned crystals in chondrules and Si-rich glass demonstrate that chondrules were not at equilibrium but experienced fractional crystallization. In perfect fractional crystallization, the most primitive olivine cores are in equilibrium with the bulk liquid, as assumed above and by Alexander et al. (2008b), while with equilibrium crystallization crystals are in equilibrium with interstitial liquid.

Table 6
Comparison of calculated equilibrium (Mathieu, 2009) and observed Type II chondrule olivine–liquid Na partition coefficients.

Chondrule	Type	FeO Oliv	Na_2O Oliv	Na_2O Liq	Equil D_{Na}	Obs D_{Na}	Obs D_{Na} s.d.	Na_2O Equil	Equil/Obs Na_2O liq
Cores–bulks									
6	IIA	11.00	0.0055	0.88	0.0023	0.0063	0.0007	2.38	2.7
20	IIA	11.74	0.0067	1.06	0.0024	0.0063	0.0006	2.80	2.6
98	IIA	16.28	0.0140	1.07	0.0029	0.0131	0.0006	4.84	4.5
101	IIA	8.62	0.0044	1.75	0.0020	0.0025	0.0003	2.15	1.2
13–36	IIA	15.04	0.0102	0.79	0.0028	0.0129	0.0008	3.70	4.7
64–65	IIA	11.91	0.0069	0.82	0.0024	0.0084	0.0007	2.86	3.5
89–90	IIA	9.55	0.0067	1.33	0.0022	0.0080	0.0005	3.12	2.3
21–22	IIA(B)	11.10	0.0030	0.94	0.0023	0.0032	0.0006	1.29	1.4
99	IIA(B)	9.40	0.0058	0.79	0.0021	0.0074	0.0007	2.72	3.5
108	IIA(B)	8.56	0.0022	0.72	0.0020	0.0031	0.0008	1.08	1.5
4	IIAB	10.14	0.0026	0.72	0.0022	0.0036	0.0008	1.17	1.6
9	IIAB	15.31	0.0053	1.35	0.0028	0.0039	0.0004	1.90	1.4
51–52	IIAB	11.21	0.0027	0.75	0.0023	0.0036	0.0004	1.16	1.5
Rims–glasses									
64–65	IIA	22.86	0.0220	6.99	0.0036	0.0031	0.0008	6.09	0.9
89–90	IIA	24.86	0.0195	5.16	0.0038	0.0038	0.0002	5.09	1.0
98	IIA	20.68	0.0260	8.61	0.0034	0.0030	0.0008	7.70	0.9
122	IIA	30.03	0.0228	6.02	0.0044	0.0038	0.0004	5.18	0.9
8	IIA(B)	23.71	0.0164	8.86	0.0039	0.0018	0.0002	4.23	0.5
99	IIA(B)	19.72	0.0140	8.33	0.0033	0.0017	0.0002	4.28	0.5
51–52	IIAB	22.00	0.0175	8.02	0.0035	0.0022	0.0002	4.97	0.6

Calculated liquidus olivine calculated using PETROLOG are more magnesian than the most primitive observed olivine cores, suggesting a departure from perfect fractional crystallization in Semarkona Type II chondrules. Flat zoning profiles in the centers of olivine crystals (Jones, 1990; Miyamoto et al., 2009; Hewins, 2009) also indicate an approach to equilibrium crystallization (crystal–liquid exchange) at the highest temperatures.

Libourel (1999) examined the nature of crystallization of Semarkona Type II chondrules by comparing their olivine-melt partition coefficients for CaO corrected for bulk composition effects, D^*_{CaO}, to those measured experimentally. He found that Semarkona chondrule assemblages were not at equilibrium and, for *average* olivine compositions (Jones, 1990) and mesostasis compositions, D^*_{CaO} falls about 1 log unit below the equilibrium values. Evaluating our data with olivine-melt Ca partitioning, we observe that for the most primitive core compositions and liquids of bulk chondrule composition D^*_{CaO} falls between the equilibrium values defined by Libourel and 1 log unit higher (1999). For the data set with the best statistics (Alexander et al., 2008b), 15 of 20 rim-glass pairs and 10 of 18 core-bulk pairs have D^*_{CaO} values within 1/2 log unit of the equilibrium curve (Libourel, 1999), Where our mesostasis is Ca-rich, D^*_{CaO} for rims have lower than equilibrium values, related probably to crystallization of Ca-rich pyroxene. Thus olivine and melt had close to equilibrium Ca partitioning in Semarkona Type II chondrules and, in particular, interface equilibrium unmodified by diffusion was maintained for Ca as for Na during the late fractionation of olivine.

We reconsider the possibility (Fig. 4) that Na in core olivine was increased by diffusion during crystallization. Calcium profiles are flatter in chondrule olivine than Fe–Mg profiles (Hewins, 2009), consistent with slower diffusion of Ca, and Na and Ca have similar diffusion coefficients (Spandler et al., 2010). Olivine core Na concentrations and D_{Na} seem to be independent of bulk liquid Na compositions ($R^2 = 0.23$, Fig. 6b). We therefore have no evidence that olivine core Na concentration was diffusing into olivine from liquids enriched in Na. In addition, many inclusions have preserved low Na concentrations in conflict with such assumed Na-rich liquid compositions, suggesting that there was little enrichment of Na in olivine.

The preservation of oscillatory zoning of P in cores of olivine crystals in Type IIA chondrules (Jones, 1990; Hewins, 2009 Fig. 5b) and, to a lesser extent, of P correlated with other incompatible elements in some Type II olivine rims, plus hopper morphology and melt inclusions in many cases, indicate rapid growth. It is possible that elements other than P, e.g. Na, were enriched in cores, or in concentric zones, shortly after crystallization began, because of the presence of the liquid boundary layer responsible for the P zonation. However, Na diffuses faster than P though slower than Fe–Mg (Qian et al., 2010; Spandler and O'Neill, 2010) and its profiles are smooth, so no evidence of rapid growth generating high Na persists. It is, however, possible that Na and other relatively rapidly diffusing incompatible elements were redistributed from such rapidly grown zones. The fact that Fe–Mg diffusion has not destroyed relict forsteritic cores indicates limits to such diffusion.

Bulk composition effects other than the FeO influence on Na partitioning can be considered. Type IIA chondrules have higher P concentrations (mean 0.33, s.d. 0.19 wt.% P_2O_5) than IIA(B)-AB (mean 0.06, s.d. 0.04% wt.% P_2O_5), a significant difference at the 95% confidence level. The highest Na contents of olivine cores are associated with the most P-rich chondrules (Tables 1 and 4). These are the chondrules showing concentric P zoning in olivine, so

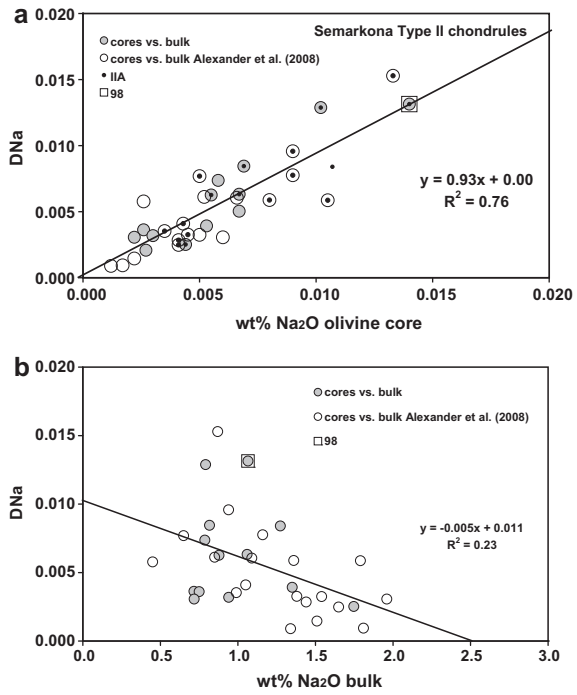

Fig. 6. Na partition coefficient for olivine cores vs. bulk liquid. (a) Correlation with Na in olivine cores. (b) No significant correlation with Na in bulk melt. Data from this study and Alexander et al. (2008b).

there might have been enhanced incorporation of Na and other incompatible elements along with P. However, it is difficult to see why IIA chondrules should have experienced rapid growth of olivine from boundary layers and not IIAB-IIA(B) chondrules. They have similar cooling rates and Type IIA(B) chondrules have the highest liquidus temperatures. We conclude that diffusion may have played some role in the presence of high Na in olivine cores and that the liquid concentrations predicted from D_{Na} assuming equilibrium are best regarded as upper limits.

4.3. Na variation with time and chondrule formation

Prior to analysis of melt inclusions and knowledge of the FeO dependence of D_{Na} it was argued that chondrules were essentially closed systems with respect to Na (Borisov et al., 2008; Alexander et al., 2008b). This would give a steady increase in Na concentration in residual liquid during chondrule crystallization, but we infer a decrease followed by an increase. Olivine core Na concentrations suggest that chondrule initial melts were more Na-rich than present chondrule bulk compositions; Na in melt inclusions in olivine that the liquids lost Na during olivine crystallization; and Na in mesostases that Na was augmented over levels due to fractional crystallization alone. Even though the high concentrations of moderately volatile elements indicate that Type II chondrules may have formed in a high density region, there is still evidence of at least partially open system behavior. We used equilibrium D_{Na} to calculate original equilibrium initial liquid Na concentrations and modeled open system crystallization of such initial liquids so as to match inclusion and mesostasis compositions. This model suggests that Type IIAB chondrules have evaporated close to half their Na, but regained most of it. Type IIA chondrules would have lost more than half their Na, provided redistribution of Na within the olivine was not extensive, and recondensation was incomplete. For IIAB chondrules, the near equilibrium D_{Na} values confirm that there has been little net change in Na, as they have recovered most of the lost Na. For IIA chondrules, however, the olivine-melt data indicate that the chondrules have significantly less Na than their precursors, which is not unreasonable considering the large losses and gains found during heating and cooling in the calculations of Fedkin et al. (2011). Lower amounts of evaporation for Type IIAB than for Type IIA chondrules might be related to the higher viscosity of the former when molten (Yu and Hewins, 1998). However, the higher model losses for IIA chondrules than for IIAB chondrules, based on D_{Na} values, are also explained if both approached equilibrium with the same ambient gas at peak temperatures. Those chondrules with higher initial Na, i.e. mostly Type IIA as indicated by their higher Na in olivine, would need to experience more initial evaporation to reach equilibrium with the gas composition reached after heating.

An alternative interpretation of primitive olivine cores which are Na-rich is that they were not crystallized from the bulk chondrule liquid. If there are large quantities of unrecognized relict grains, the liquid from which the most primitive grains we analyzed grew could have been less olivine-normative than the bulk composition, and we would have overestimated the initial Na content somewhat. If the most primitive grains with relatively high Na are relict grains, they suggest early Na-rich chondrule melts. We have no evidence for or against this idea, but note that if these compositions are relict grains, they would be consistent with evaporation of earlier chondrule melts to give the present chondrule precursors and parental liquids.

Some IIA chondrules have bulk SiO_2 contents similar to those of Mg-rich olivine so that daughter liquids cannot concentrate SiO_2 until the fractionating olivine becomes more ferroan. This results in calculated final liquids that are less Si-rich than observed mesostases, and raises the possibility of condensation of SiO into Type II chondrule melts, as suggested by Villeneuve (2010). Condensation of SiO into Type I chondrule melts has been demonstrated by Tissandier et al. (2002) and Libourel et al. (2006), and Jones (1994) showed that mesostasis of Semarkona Type IAB chondrules is more Si-rich than that of type IA chondrules. Hewins and Zanda (in press) have discussed open system behavior for Si, Fe, Mn and S in Type I and II chondrules. Mathieu (2009) has shown that the solubility of Na in CMS melts increases with the SiO_2 content (see also Mathieu et al., 2011), and he suggested that the condensation of SiO into chondrule melts would be followed by enhanced Na condensation. However, neither bulk nor mesostasis compositions show significantly different mean Na_2O concentrations in Type IIA, IIAB and IIB chondrules (e.g. Jones, 1990, 1996) despite the major differences in

SiO_2. The standard deviations of Na_2O concentrations in these mesostases are, however, larger than the differences predicted by Mathieu (2009) between Type IIA and IIAB liquids coexisting with olivine. In the context of the particle-vapor clump model (Hewins, 1989; Cuzzi and Alexander, 2006), this suggests great variations of vapor composition or cooling time.

Under conditions where Na evaporation and recondensation are extensive, some loss and recondensation of Fe and Si are likely (e.g. Villeneuve, 2010; Fedkin et al., 2011). Differences in compositions of Type II chondrule olivines in CM and OC chondrites can be explained in terms of recondensation in different environments (Hewins et al., 2011). Open-system behavior of Fe and Si would modify the details of crystallization, and influence the evolution of the Na concentrations. If Type II chondrules did behave as open systems, the absence of isotopic mass fractionations, of K (e.g. Alexander et al., 2000), Fe and Si becomes a major constraint. It suggests isotopic exchange between gas and liquid over periods of hours so that chondrule liquids could approach equilibrium silicate melt compositions (Alexander, 2004; Cuzzi and Alexander, 2006).

Based on experiments at 1 atm, retention of Na in Type II chondrule liquids requires a local gas enriched in ice and dust component by 100x or 1000x solar composition, respectively (Yu and Hewins, 1998). Chondrules require higher than canonical pressures to prevent evaporation of metallic iron (Cohen and Hewins, 2004) and chondrules which experienced any FeO evaporation would have lost all their alkalis (Cohen et al., 2004). These inferences from simple experiments that chondrules require non-canonical conditions during formation to explain their Na and FeO are supported by recent calculations. Fedkin et al. (2011) extended the approach of Desch and Connolly (2002) to the model of chondrule formation by gas shocks, by modeling the evaporation and recondensation of such components at P_T of $\sim 10^{-5}$ atm with large dust and ice enrichments, and by calculating the extent of olivine fractionation and isotopic mass fractionation. They showed total loss of Na, K, Fe and Ni, and partial losses of Si and Mg at peak conditions, depending in detail on heating rates and peak temperatures assumed. Allowing complete evaporation of Na, rather than ~10% (Alexander et al., 2008a,b), relaxes the necessary dust enrichment by an order of magnitude. Nevertheless, differences in calculated and observed olivine Fa histograms, and especially isotopic fractionations of several ‰, found in the simulations of Fedkin et al. (2011) require extreme conditions of total pressure and dust-ice enrichment. Very high P_T has already been suggested to explain chondrule Mg isotopic data (Galy et al., 2000) though Cuzzi and Alexander (2006) considered that overlapping evaporation clouds from many adjacent chondrules would be sufficient.

The high (apparent) D_{Na} values for olivine cores are best explained by evaporation of Na at peak temperatures, leaving fossil Na-rich olivine in liquids impoverished in Na. This evaporation also explains lower Na contents in melt inclusions than expected from fractional crystallization calculations for bulk compositions enriched in Na by late recondensation into mesostasis. Yet our Na contents of olivine, cores and rims, are always significantly greater than zero in high-precision long-duration analyses (Fig. 2a), as are those of Alexander et al. (2008b), i.e. there is no record of a stage of total evaporation of Na. Our calculated Na losses are modest relative to those expected for canonical low ambient partial pressures consistent with the conclusions of Fedkin et al. (2011) that higher than canonical pressures and high dust-ice enrichments are required.

High P_{Na} and incomplete Na evaporation confirm that there were very high particle densities in the regions or clumps where chondrules were forming (Hewins, 1989, 1991; Yu et al., 2003; Alexander et al., 2008b), and imply that collisions of molten chondrules should have been frequent. Wasson et al. (1995) estimated that 2.4% of chondrules in ordinary chondrites are compound chondrules. Given an interval of at least 600 °C between their liquidus and glass transition temperatures and cooling rates ~1–1000 °C/hr (Hewins et al., 2005; Miyamoto et al., 2009), chondrules would be sticky for hours. Alexander et al. (2008a,b) estimated the number density of chondrules to be about 10,000 per m^3, with evaporation of Na limited to ~10%. Here we see evidence for greater loss of Na, meaning the true number density is somewhat less. Still it is initially very surprising, given number density and long cooling time, that compound chondrules are not more abundant than 2.4% of all chondrules. However, in many ordinary chondrites, including Semarkona, the chondrules actually aggregated into clusters (Zanda, 2004). The aggregation must have been slow enough for Semarkona that chondrules cooled normally and diffusion did not erase igneous zoning in olivine. Such chondrites with a second kind of primary accretion texture, distinct from that in CM chondrites, may be described as cluster chondrites (Metzler, 2011). Thus some chondrules began to accrete while hot, as clusters formed before accretion (because of channels filled with matrix separating them), and/or directly to the parent body surface (Hutchison et al., 1979). These clusters also offer strong support for a high number density of chondrules.

We infer greater Na loss than Alexander et al. (2008b) and, though this requires a little less dust enrichment, we find no record of the zero condensed Na stage required for heating at nebular pressures (Fedkin et al., 2011). A rather extreme modification of canonical conditions is still required. The high P_T and dust-ice enrichment required, and their consequences for chondrule compositions, are more easily explained by collision of icy protoplanets than by nebular concentration mechanisms (Fedkin et al., 2011). Relict grains with high dislocation densities had previously been explained by chondrule formation in collisions of comet-like grandparent bodies (Kitamura and Tsuchiyama, 1991). Asphaug et al. (2011) recently modeled chondrule formation as a result of collision of small molten planetesimals, though they did not discuss the presence of metal and sulfide in chondrules. Alternatively collisions of much larger undifferentiated bodies resulting in melting would explain the presence of dense metal-sulfide liquids in silicate melt droplets.

Chondrule melting and clustering in dense clumps either in the disk or in a collision debris cloud would probably have contributed to rapid accretion. Turbulent

concentration can produce large concentrations of chondrule-sized particles in the disk and, if sufficiently large, these clumps are self-gravitating (Cuzzi et al., 2008; Alexander et al., 2008a). However, collisions of protoplanets could also rapidly produce high density clouds of melted particles. High P_{Na} and the formation of clusters of chondrules in these swarms are easily understood. With turbulent concentration in the disk (Cuzzi et al., 2008), the chondrule clumps would have accumulated into new asteroidal bodies. With oblique collisions, many chondrules could be reaccreted on the remnants of the grandparent body in a matter of hours, and some downrange chondrule spray could form self-gravitating clumps leading to new parent bodies (Asphaug et al., 2011). Clusters in Semarkona, formed as rocklets like multiple compound chondrules by random collisions in the expanding plume, would have cooled as they formed because there is no metamorphic diffusion in the olivine crystals. Similar textures might form with chondrules falling back onto the remains of the target, provided they accumulated slowly enough to cool rapidly in the sub-solidus. Alternatively, with abundant and rapid accumulation, the fallback might form a hot blanket. Then we have the intriguing possibility of equilibrated and unequilibrated chondrites forming as the result of the same event, but on (grand)parent and reassembled daughter bodies of fundamentally different character.

5. CONCLUSIONS

The distribution of Na between melt and olivine in chondrules yields information on changes in P_{Na} in ambient gas. The different Na concentrations preserved in Semarkona Type II chondrule bulk liquids, melt inclusions and mesostases are broadly consistent with fractional crystallization of olivine, ± pyroxene. However, glass inclusions in olivine have lower Na than expected compared to calculated daughter liquids, and mesostasis has higher, which is consistent with evaporation followed by condensation of Na into melt not enclosed within olivine.

The most primitive olivine cores in each chondrule are mostly between Fa_8 and Fa_{13}, with 0.0022–0.0069 ± 0.0013 wt.% Na_2O. IIAB chondrule olivine core compositions have consistently lower Na contents than IIA olivine cores. Extreme rim compositions are $\sim Fa_{35}$ and 0.03 wt.% Na_2O.

Chondrule olivine rims are close to being in equilibrium with the mesostasis with respect to Na and Ca contents. Olivine cores, particularly in IIA chondrules, have very high D_{Na} due to incorporation of high concentrations of Na in the early olivine. This is compatible with evaporation of Na from the melt at peak temperatures, consistent with the low Na contents of the glass inclusions, and only partial recondensation of the lost Na into mesostasis melt.

The high P_{Na} required for these chondrules suggests very high particle densities during chondrule formation, either in clumps in the disk or in debris clouds resulting from collisions of protoplanetary bodies. The particle densities are consistent with the observation that chondrules actually aggregated into clusters before incorporation in Semarkona and the idea that accretion proceeded rapidly after chondrule formation.

ACKNOWLEDGEMENTS

We thank Frédéric Couffignal and Michel Fialin of Université Paris VI, and Jean-Luc Devidal of Université Blaise Pascal, for invaluable assistance during microprobe work. Omar Boudouma (Université Paris VI) helped us with BSE cartography. Ken Koga Université Blaise Pascal) performed chondrule crystallization calculations using MELTS, which showed very similar results to those of PETROLOG. Paul Warren kindly gave us his worksheet for density corrections for bulk rock EMP analysis, which we adapted for chondrules. Conel Alexander and Andreas Pack made useful comments on an early version of this manuscript. We thank Romain Mathieu and an anonymous reviewer for thorough critical reading of the text, which resulted in many improvements, and Jeff Cuzzi for helpful discussions. We are grateful to MNHN Paris for the Semarkona sections ns1 and ns2. Financial support was provided by ANR (no. 07-BLAN-0130-04 "MIME" B. Zanda), by the French PNP program (B. Zanda), a Fulbright US Student Fellowship 03084064 (Claire Bendersky), and NASA Cosmochemistry Grants NNG05GK11G and. NNX08AG62G.

REFERENCES

Alexander C. M. O'D. (2004) Chemical equilibrium and kinetic constraints for chondrule and CAI formation conditions. *Geochim. Cosmochim. Acta* **68**, 3943–3969.

Alexander C. M. O'D., Grossman J. N., Wang J., Zanda B., Bourot-Denise M. and Hewins R. H. (2000) The lack of potassium isotopic fractionation in Bishunpur chondrules. *Meteorit. Planet. Sci.* **35**, 859–868.

Alexander C. M. O'D., Grossman J. N. and Ebel D. (2007) Do we need to reassess the formation conditions of chondrules? *Lunar Planet. Sci. XXXVII*. #2012 (abstr.).

Alexander C. M. O'D., Ebel D. S., Ciesla F. and Grossman J. N. (2008a) Reassessing the conditions of chondrule formation. *Lunar Planet. Sci. XXXIX*. #2440 (abstr.).

Alexander C. M. O'D., Grossman J. N., Ebel D. S. and Ciesla F. J. (2008b) The formation conditions of chondrules and chondrites. *Science* **320**, 1617–1619.

Ariskin A. A., Frenkel M. Ya., Barmina G. S. and Nielsen R. (1993) COMAGMAT: a Fortran program to model magma differentiation processes. *Comput. Geosci.* **19**, 1155–1170.

Asphaug E., Martin J. and Movshovitz N. (2011) Chondrule formation by partial accretion of planetesimals. *Lunar Planet. Sci. XLII*. #1647 (abstr.).

Borisov A., Pack A., Kropf A. and Palme H. (2008) Partitioning of sodium between olivine and melt: an experimental study with application to the formation of meteoritic Na-rich chondrule glass and refractory forsterites. *Geochim. Cosmochim. Acta* **72**, 5558–5573.

Chaussidon M., Libourel G. and Krot A. (2008) Oxygen isotopic constraints on the origin of magnesian chondrules and on the gaseous reservoirs in the early Solar System. *Geochim. Cosmochim. Acta* **72**, 1924–1938.

Cohen B. A. and Hewins R. H. (2004) An experimental study of the formation of metallic iron in chondrules. *Geochim. Cosmochim. Acta* **68**, 1677–1689.

Cohen B. A., Hewins R. H. and Alexander C. M. O'D. (2004) The formation of chondrules by open-system melting of nebular condensates. *Geochim. Cosmochim. Acta* **68**, 1661–1675.

Cuzzi J. N. and Alexander C. M. O'D. (2006) Chondrule formation in particle-rich nebular regions at least hundreds of kilometres across. *Nature* **441**, 483–485.

Cuzzi J. N., Hogan R. C. and Shariff K. (2008) Toward planetesimals: dense chondrule clumps in the protoplanetary nebula. *Astrophys. J.* **687**, 1432–1447.

Danyushevsky L. V. (2001) The effect of small amounts of H_2O on crystallization of mid-ocean ridge and back-arc basin magmas. *J. Volc. Geotherm. Res.* **110**, 265–280.

Danyushevsky L. V. and Plechov P. (2011) Petrolog3: integrated software for modeling crystallization processes. *Geochem. Geophys. Geosyst.* **12**, Q07021. doi:10.1029/2011GC003516.

Desch S. J. and Connolly, Jr., H. C. (2002) A model for the thermal processing of particles in solar nebula shocks: application to cooling rates of chondrules. *Meteorit. Planet. Sci.* **37**, 183–208.

Ebel D. S. and Grossman L. (2000) Condensation in dust-enriched systems. *Geochim. Cosmochim. Acta* **64**, 339–366.

Faure F. and Schiano P. (2005) Experimental investigation of equilibration conditions during forsterite growth and melt inclusion formation. *Earth Planet. Sci. Lett.* **236**, 882–898.

Faure F., Schiano P., Trolliard G., Nicollet C. and Soulestin B. (2007) Textural evolution of polyhedral olivine experiencing rapid cooling rates. *Contrib. Mineral. Petrol.* **153**, 405–416.

Fedkin A. V., Grossman L., Ciesla F. J. and Simon S. B. (2011) Mineralogical and isotopic effects of shock wave thermal histories on chondrule precursors. *Lunar Planet. Sci. XLII*, #1834 (abstr.).

Galy A., Young E. D., Ash R. D. and O'Nions K. (2000) The formation of chondrules at high gas pressures in the solar nebula. *Science* **290**, 1751–1753.

Grant K. J. and Wood B. J. (2010) Experimental study of the incorporation of Li, Sc, Al and other trace elements into olivine. *Geochim. Cosmochim. Acta* **74**, 2412–2428.

Hewins R. H. (1989) The evolution of chondrules. *Proc. NIPR Symp. Antarct. Meteorites* **2**, 202–222.

Hewins R. H. (1991) Retention of sodium during chondrule melting. *Geochim. Cosmochim. Acta* **55**, 935–942.

Hewins R.H. (2009) Minor Element Zoning of Olivine in Type IIA Chondrules in Semarkona. *Lunar Planet. Sci. XL*. #1669 (abstr.).

Hewins R. H. and Zanda B. (in press) Chondrules: precursors and interactions with the nebular gas. *Meteorit. Planet. Sci.* **47**.

Hewins R. H., Connolly H. C. Jr., Lofgren G. E. and Libourel G. (2005) Experimental constraints on chondrule origins. In *Chondrites And the Protoplanetary Disk. ASP Conference Series 341* (eds. A. N. Krot, E. R. D. Scott and B. Reipurth). Astronomical Society of the Pacific, San Francisco. pp. 286–317

Hewins R. H., Ganguly J. and Mariani E. (2009a) Diffusion modeling of cooling rates of relict olivine in Semarkona chondrules. *Lunar Planet. Sci. XL*. #1513 (abstr.).

Hewins R. H., Zanda B., Bendersky C. and Leroux H. (2009b) Evolution of melt compositions in Semarkona type II chondrules. *Meteorit. Planet. Sci.* **43**, A89, #5279.

Hewins R. H., Zanda B. and Bourot-Denise, M. (2011) The formation of Type II chondrules in CM chondrites: The view from Paris. *Lunar Planet. Sci. XLII*. #1914 (abstr.).

Humayun M. and Clayton R. N. (1995) Potassium isotope cosmochemistry: genetic implications of volatile element depletion. *Geochim. Cosmochim. Acta* **59**, 2131–2148.

Hutchison R., Bevan A. W. R., Agrell S. O. and Ashworth J. R. (1979) Accretion temperature of the Tieschitz, H3, chondritic meteorite. *Nature* **280**, 116–119.

Jones R. H. (1990) Petrology and mineralogy of Type II, FeO-rich chondrules in Semarkona LL3.0: origin by closed-system fractional crystallization, with evidence for supercooling. *Geochim. Cosmochim. Acta* **54**, 1785–1802.

Jones R. H. (1994) Petrology of FeO-poor, porphyritic pyroxene chondrules in the Semarkona chondrite. *Geochim. Cosmochim. Acta* **158**, 5325–5340.

Jones R. H. (1996) FeO-rich porphyritic pyroxene chondrules in unequilibrated ordinary chondrites. *Geochim. Cosmochim. Acta* **60**, 3115.

Jones R. H. and Lofgren G. E. (1993) A comparison of FeO-rich, porphyritic olivine chondrules in unequilibrated chondrites and experimental analogues. *Meteoritics* **28**, 213–221.

Kitamura M. and Tsuchiyama A. (1991) icy grandparent bodies for shock origin of ordinary chondrites. *Lunar Planet. Sci. Conf. XXII*, 723–724.

Kropf A. (2009) Alkalien in chondren – offenes oder geschlossenes system? Dissertation Dr. rer. nat., Georg-August-Universität, Göttingen.

Libourel G. (1999) Systematics of calcium partitioning between olivine and silicate melt: implications for melt structure and calcium content of magmatic systems. *Contrib. Mineral. Petrol.* **136**, 63–80.

Libourel G. and Krot A. N. (2007) Evidence for the presence of planetesimal material among the precursors of magnesian chondrules of nebular origin. *Earth Planet. Sci. Lett.* **254**, 1–8.

Libourel G., Krot A. N. and Tissandier L. (2006) Role of gas-melt interaction during chondrule formation. *Earth Planet. Sci. Lett.* **251**, 232–240.

Mathieu R. (2009) Solubilité du sodium dans les silicates fondues. Ph. D. thesis, INPL-CRPG Nancy.

Mathieu R., Libourel G., Deloule E., Tissandier L., Rapin C. and Podor R. (2011) Na_2O-solubility in molten CaO–MgO–SiO_2 system. *Geochim. Cosmochim. Acta* **75**, 608–628.

McCanta M. C., Beckett J. R. and Stolper E. M. (2008) Zonation of phosphorus in olivine: dynamic crystallization experiments and a study of chondrule olivine in unequilibrated ordinary chondrites. *Lunar Planet. Sci. XXXIX*. #1807.

McSween, Jr., H. Y. (1977a) Chemical and petrographic constraints on the origin of chondrules and inclusions in carbonaceous chondrites. *Geochim. Cosmochim. Acta* **41**, 1843–1860.

McSween, Jr., H. Y. (1977b) On the nature and origin of isolated grains in carbonaceous chondrites. *Geochim. Cosmochim. Acta* **41**, 411–418.

Metzler K. (2011) Chondrite accretion within hours to a few days after chondrule formation? Textural evidence from UOCs. LPI Workshop on Formation of the First Solids in the Solar System. Poipu Beach, Hawai'i. #9111 (abstr.).

Miyamoto M., Mikouchi T. and Jones R. H. (2009) Cooling rates of porphyritic olivine chondrules in the Semarkona LL3.00 ordinary chondrite: a model for diffusional equilibration of olivine during fractional crystallization. *Meteorit. Planet. Sci.* **44**, 521–530.

Morgan G. B. V. I. and London D. (2005) The effect of current density on the electron microprobe analysis of alkali aluminosilicate glasses. *Am. Mineral.* **90**, 1131–1138.

Qian Q., O'Neill H. St. and Hermann J. (2010) Comparative diffusion coefficients of major and trace elements in olivine at ~950 °C from a xenocryst included in dioritic magma. *Geology* **38**, 331–334.

Sack R. O., Carmichael I. S. E., Rivers M. L. and Ghiorso M. S. (1980) Ferric-ferrous equilibria in natural silicate liquids at 1 bar. *Contrib. Mineral. Petrol.* **75**, 369–376.

Scott E. R. D. and Taylor G. J. (1983) Chondrules and other components in C, O, and E chondrites: similarities in their properties and origins. *Proc. Lunar Planet. Sci. Conf.* **14**, B275–B286.

Spandler C. and O'Neill H. St. C. (2010) Diffusion and partition coefficients of minor and trace elements in San Carlos olivine at

1,300 °C with some geochemical implications. *Contrib. Mineral. Petrol.* **159**, 791–818.

Tissandier L., Libourel G. and Robert F. (2002) Gas-melt interactions and their bearing on chondrule formation. *Meteorit. Planet. Sci.* **37**, 1377–1389.

Tronche E. (2007) Formation du système solaire: nouvelles données sur l'histoire thermique des chondres et inclusions réfractaires. Ph. D. thesis, MNHN Paris.

Villeneuve J. (2010) Formation des chondres: précurseurs et chronologie. Ph. D. thesis, INPL-CRPG Nancy.

Warren P. H. (1997) The unequal host-phase density effect in electron probe defocused beam analysis: an easily correctable problem. *Lunar Planet. Sci. XXVIII*. #1406 (abstr.).

Wasson J. T., Krot A. N., Lee M. S. and Rubin A. E. (1995) Compound chondrules. *Geochim. Cosmochim. Acta* **59**, 1847–1869.

Whattam S. A. and Hewins R. H. (2009) An origin for PO chondrules from thermally annealed granoblastic olivine aggregates. *Geochim. Cosmochim. Acta* **73**, 5460–5482.

Yu Y. and Hewins R. H. (1998) Transient heating and chondrule formation – evidence from Na loss in flash heating simulation experiments. *Geochim. Cosmochim. Acta* **62**, 159–172.

Yu Y., Hewins R. H., Alexander C. M. O'D. and Wang J. (2003) Experimental study of evaporation and isotopic mass fractionation of potassium in silicate melts. *Geochim. Cosmochim. Acta* **67**, 773–786.

Zanda B. (2004) Chondrules. *Earth Planet. Sci. Lett.* **224**, 1–17.

Zanda B., Bourot-Denise M., Perron C. and Hewins R. H. (1994) Origin and metamorphic redistribution of silicon, chromium and phosphorus in the metal of chondrites. *Science* **265**, 1846–1849.

Associate editor: Christian Koeberl